Evidence for Phagocytosis of Apoptotic Bodies by Microglial Cells

Immunohistochemical findings demonstrated that activation and infiltration of microglial cells occurred in the SVZ and RMS of MPTP-treated mice. Marked increases in the number of Iba 1^+ cells were observed in the SVZ (Fig. 4A) and RMS (Fig. 5A). The peak in the number of microglial cells in the SVZ was observed at 24 hours after MPTP injection (Fig. 4B), paralleling that of apoptotic cells and suggesting the increase in microglial cells is a response to MPTP-induced apoptosis. Activated microglial cells were clearly observed in the RMS (Fig. 5B). Ultrastructural analysis demonstrated that the phagocytosis of apoptotic bodies by microglial cells occurred in the SVZ (Fig. 4C) and RMS (Fig. 5C) in MPTP-treated mice. Findings of TUNEL and Iba 1 double-labeling as shown in Figures 4D and 5D indicated that TUNEL-positive nuclei were enveloped by Iba 1^+ cells, supporting the occurrence of phagocytosis.

Phenotype of Cells Undergoing Apoptosis in the Subventricular Zone and Rostral Migratory Stream

Figures 6A and 6B show that the majority of cells expressing Dcx (a marker for migrating neuroblasts, A cells) are positive for cleaved caspase-3 in the SVZ (Fig. 6A) and RMS (Fig. 6B). A few cells expressing cleaved caspase-3 were also stained with GFAP (a marker for astrocytes, B cells) (SVZ, Fig. 6C; RMS, Fig. 6D). No $EGFR^+$ (SVZ, Fig. 6E; RMS, Fig. 6F) or LeX^+ cells (SVZ, Fig. 6G; RMS, Fig. 6H) were observed to express cleaved caspase-3. It has been demonstrated that the $EGFR^+/GFAP^-$ or $LeX^+/GFAP^-$ cells corresponded to transit-amplifying, multipotent type C cells in the adult SVZ, and some C cells were also found in the RMS (18, 34). Although a small subset of B cells expressed EGFR, they apparently were in contact with the lateral ventricle (18). Cleaved caspase-3 was not expressed by any C cells.

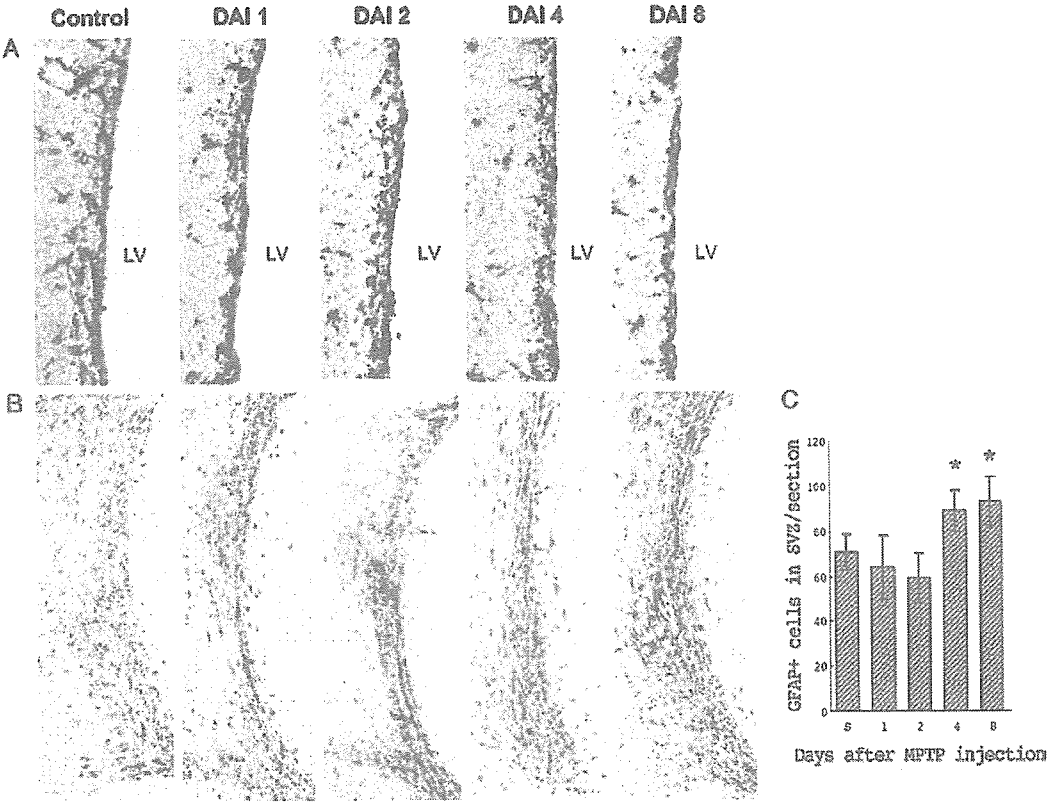

FIGURE 8. Changes in the number of $GFAP^+$ astrocytes after MPTP injection in the subventricular zone (SVZ) and rostral migratory stream (RMS). Representative microphotographs of coronal and sagittal sections immunostained for GFAP in the SVZ (A) and RMS (B) obtained from MPTP-treated mice killed at 1, 2, 4, and 8 days after injection. Controls received saline only. Scale bars = (A) 50 μm; (B) 100 μm. No change was observed at day 2, whereas a significant increase in numbers of GFAP-immunoreactive astrocytes was noted at 4 and 8 days after MPTP administration compared with the control (C). Data are expressed as means ± standard error of mean. *, $p < 0.05$ compared with saline. The numbers of $GFAP^+$ cells in the unilateral SVZ were counted in 3 to 5 different brains. S, saline control; LV, lateral ventricle.

To validate the findings of cleaved caspase-3 double-labeling with cell markers, we performed an ultrastructural analysis. Distinct cell types were identified according to the criteria defined by Doetsch et al (19). As shown in Figures 3A and 3B, cells that were in the early stage of apoptotic death exhibited the ultrastructural characteristics of A cells: an open pericellular space, a scant and dark cytoplasm, and smooth contours. Cells that were at an advanced stage of apoptotic death were observed adjacent to A cells (Fig. 3B, C, E, F, a), located close to C cells. C cell has an irregular nucleus with deep invaginations and mostly lax chromatin and has a typical, large reticulated nucleolus (Fig. 3A, B, E, F, c). These observations together with the findings of cleaved caspase-3 double-staining suggest that the majority of cells undergoing apoptosis are A cells, that is, migrating neuroblasts.

Dcx+ Cell Numbers Are Decreased After MPTP Injection

The occurrence of apoptosis in A cells is thought to be followed by a loss of A cells. To test this hypothesis, we labeled brain sections with antibody against Dcx, a marker of migrating neuroblasts. In the SVZ, there was a 65.2%, 37.1%, and 24.3% reduction of A cells at 2, 4, and 8 days after MPTP injection, respectively (Fig. 7A, C). The same changes were also observed in the RMS (Fig. 7B). $GFAP^+$ B cell number were not significantly reduced at any time point, indicating apoptotic death occurred in very few B cells (Fig. 8). We also observed a significant (26.2% and 31.9%) increase in B cells in the SVZ at 4 and 8 days after MPTP injection, respectively (Fig. 8A, C). This may be the result of a response to the loss of A cells.

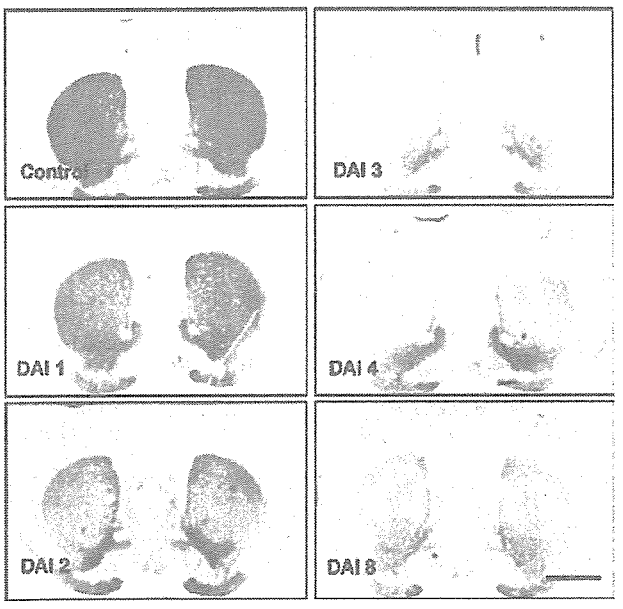

FIGURE 9. Representative coronal sections through striatum were immunostained for tyrosine hydroxylase (TH) and visualized with DAB showing the reduction of TH-immunoreactive fibers by 1, 2, 3, 4, and 8 days after MPTP injection (DAI). The largest reduction was found by DAI 3 and DAI 4 compared with saline controls. Scale bar = 1.5 mm.

Reduction of Dopaminergic Fibers in Striatum

To determine whether the MPTP regimen used here simultaneously produces striatal dopamine depletion, we performed an immunohistochemistry study with an antibody raised against tyrosine hydroxylase (TH), the rate-limiting enzyme in the synthesis of dopamine. MPTP-treated mice exhibited patterns of TH-immunoreactive fiber loss (Fig. 9), which was particularly apparent at 3 and 4 days after MPTP lesion when compared with saline control.

DISCUSSION

In the present study, a single injection of MPTP produced a rapid and profound loss in dopaminergic fibers (TH-immunoreactive) in the striatum at day 1, which was maximal at 3 and 4 days after MPTP administration, suggesting this regimen could also induce biochemical changes in nigral–striatal dopamine system similar to the findings with other regimens such as acute or subacute regimen.

This study is the first to demonstrate that a single injection of MPTP-induced apoptotic cell death in the SVZ and RMS in a mouse model of PD. The cell death was observed 12 to 48 hours after an intraperitoneal injection with a peak at 24 hours as detected by TUNEL and immunohistochemistry for cleaved caspase-3. Ultrastructural findings supported the occurrence of apoptosis in the SVZ and RMS. The majority of cells dying in the SVZ and RMS were Dcx-immunoreactive migrating neuroblasts. A few were GFAP-immunoreactive and identified as astrocytes. Cells expressing cleaved caspase-3 were not labeled with EGFR or LeX. Furthermore, the present study demonstrated that MPTP-induced apoptosis was followed by a 65.2%, 37.1%, and 24.3% reduction in the number of Dcx-immunoreactive cells by 2, 4, and 8 days, respectively, confirming that the induction of apoptosis by a single dose of MPTP contributes to the loss of Dcx-immunoreactive cells (i.e. migrating neuroblasts).

The apoptosis of the cells in the SVZ and RMS is further supported by the prominent phagocytosis of fragmented DNA by microglial cells detected using a double-labeling method with TUNEL and a marker for microglial cells as well as ultrastructural analysis. TUNEL-positive microglial cells were observed throughout the cytoplasm, including the protrusions, but often had an intact nucleus, suggesting that these cells have indeed phagocytosed dying apoptotic cells in the SVZ and RMS rather than undergoing apoptosis themselves (35). Moreover, in the present study, the infiltration and activation of microglial cells in the SVZ and RMS paralleled the ongoing apoptosis. The number of microglial cells in the SVZ peaked at 24 hours and then decreased, reaching the control level at 4 days after the administration of MPTP. These observations suggest that the microglial infiltration and activation in the SVZ and RMS are partially attributable to the time course of MPTP-induced apoptosis in these areas.

Caspase-3 is one of the key executioners of apoptosis, being either partially or totally responsible for the proteolytic cleavage of many important proteins (36). In the present study, based on the findings of immunohistochemical staining for cleaved caspase-3, a time-dependent activation of caspase-3 in response to acute MPTP toxicity was observed that is consistent with the findings of the TUNEL assay, indicating that the activation of caspase-3 is correlated with the induction of apoptotic death in the SVZ and RMS. Duan et al suggested that immunohistochemical stains such as the cleaved caspase-3 stain could improve the detection and quantification of apoptosis in tissue sections compared with the TUNEL assay (37). To phenotype the apoptotic cells, we performed TUNEL double-staining, but found that the majority of TUNEL-positive cells did not express cellular markers. This could be attributable to the downregulation of markers in dying cells (38); therefore, we performed immunofluorescence double-labeling with antibody for cleaved caspase-3 and different cell markers instead of TUNEL double-staining.

The SVZ in adult mice contains 3 distinct cell types: migrating neuroblasts (type A cells), astrocytes (type B cells), and novel putative precursor cells (type C cells) (19). B cells as neural stem cells express GFAP and give rise to the rapidly dividing, transit-amplifying C cells that generate A cells (20, 39). A cells correspond to proliferating, migrating neuronal precursors (19, 40) and join an extensive tangential network of pathways for chain migration that feeds into the RMS leading to the OB (22). In the present study, the majority of cells undergoing apoptosis in the SVZ and RMS were identified as migrating neuroblasts (A cells) based on immunofluorescence double-labeling of cleaved caspase-3 and Dcx, and ultrastructural analysis. Dcx is a neuron-specific microtubule-associated protein expressed in newly mitotic neurons and has been used as a marker for migrating neuroblasts (41–43). Ultrastructural analysis in the present study shows that the cells undergoing apoptosis in the SVZ are separated by an open pericellular space. They adhered to the adjacent nonapoptotic cells that have an oval-shaped dark nucleus, scant and dark cytoplasm, smooth contours, and were morphologically similar to migrating neuroblasts according to the criteria defined by Doetsch et al (19). Moreover, both the apoptotic and nonapoptotic cells were located close to C cells, which have an irregular nucleus with deep invaginations, mostly lack chromatin, and have a typical large reticulated nucleolus. The significant and rapid decrease in the numbers of Dcx-immunoreactive cells caused by MPTP in the present study further supports that the majority of cells undergoing apoptosis were A cells. Although A cells are particularly susceptible to MPTP (in contrast with B and C cells), the cellular mechanism by which MPTP induces their apoptosis remains to be clarified.

Type A cells leave the SVZ and migrate along the RMS to the OB where they move radially away from the RMS and differentiate into granule and periglomerular neurons (21, 22, 44, 45). The decrease in the numbers of migrating neuroblasts induced by MPTP may cause an impairment of neurogenesis. However, we observed an increase in GFAP+ cells (type B cells) in SVZ at 4 and 8 days after MPTP injection. The adult neural stem cells possess a self-renewing capacity (25) and, as mentioned in the "Introduction", B cells will ultimately give rise to the migrating neuroblasts (type A cells); we thus speculated that there will be a recovery from the loss of A cells induced by MPTP. It will be interesting to further clarify 1) whether and how increased type B cells contribute to newborn A cells; and 2) whether this recovery requires long-term effort or impaired neurogenesis by MPTP is a transient event. Although an increase in type C cells was not detectable by immunohistochemical analysis at 8 days after MPTP injection (data not shown), we do not rule out the possibility that type C cells proliferate after an increase in type B cells. Further studies need to be performed with the aid of triple immunofluorescence and electron microscopic analysis (38) as well as at time points later than 8 days after MPTP injection.

In summary, although regimen-dependent differences may exist and remain to be investigated, apoptosis does occur in the SVZ and RMS in single-dose MPTP-treated mice. The majority of cells undergoing apoptosis were identified as migrating neuroblasts, although a few were astrocytes. No apoptotic death was observed in transit-amplifying C cells. As an extensively used animal model of PD, the MPTP-treated mouse provides an important tool to help researchers better evaluate and understand the pathogenesis of PD. The data demonstrated here may provide new insights into the MPTP mouse model of PD.

ACKNOWLEDGMENTS

The authors thank Akira Yasoshima for expert technical assistance in electron microscopy.

REFERENCES

1. Przedborski S, Vila M. The 1-methyl-4-phenyl-1,2,3,6-tetrahydropyridine mouse model: A tool to explore the pathogenesis of Parkinson's disease. Ann N Y Acad Sci 2003;991:189–98
2. Blum D, Torch S, Lambeng N, et al. Molecular pathways involved in the neurotoxicity of 6-OHDA, dopamine and MPTP: Contribution to the apoptotic theory in Parkinson's disease. Prog Neurobiol 2001;65:135–72
3. Tatton NA, Kish SJ. In situ detection of apoptotic nuclei in the substantia nigra compacta of 1-methyl-4-phenyl-1,2,3,6-tetrahydropyridine-treated mice using terminal deoxynucleotidyl transferase labelling and acridine orange staining. Neuroscience 1997;77:1037–48
4. Vila M, Jackson-Lewis V, Vukosavic S, et al. Bax ablation prevents dopaminergic neurodegeneration in the 1-methyl- 4-phenyl-1,2,3,6-tetrahydropyridine mouse model of Parkinson's disease. Proc Natl Acad Sci U S A 2001;98:2837–42
5. Spooren WP, Gentsch C, Wiessner C. TUNEL-positive cells in the substantia nigra of C57BL/6 mice after a single bolus of 1-methyl-4-phenyl-1,2,3,6-tetrahydropyridine. Neuroscience 1998;85:649–51; discussion 53
6. Przedborski S, Vila M. MPTP: A review of its mechanism of neurotoxicity. Clin Neurosci Res 2001;1:407–18
7. Serra PA, Sciola L, Delogu MR, et al. The neurotoxin 1-methyl-4-phenyl-1,2,3,6-tetrahydropyridine induces apoptosis in mouse nigrostriatal glia. Relevance to nigral neuronal death and striatal neurochemical changes. J Biol Chem 2002;277:34451–61
8. Dipasquale B, Mariani AM, Youle RJ. Apoptosis and DNA degradation induced by 1-methyl-4-phenylpyridinium in neurons. Biochem Biophys Res Commun 1991;181:1442–48

9. Du Y, Dodel RC, Bales KR, Jemmerson R, Hamilton-Byrd E, Paul SM. Involvement of a caspase-3-like cysteine protease in 1-methyl-4-phenylpyridinium-mediated apoptosis of cultured cerebellar granule neurons. J Neurochem 1997;69:1382–88
10. Mochizuki H, Nakamura N, Nishi K, Mizuno Y. Apoptosis is induced by 1-methyl-4-phenylpyridinium ion (MPP+) in ventral mesencephalic-striatal co-culture in rat. Neurosci Lett 1994;170:191–94
11. Itano Y, Nomura Y. 1-methyl-4-phenylpyridinium ion (MPP+) causes DNA fragmentation and increases the Bcl-2 expression in human neuroblastoma, SH-SY5Y cells through different mechanism. Brain Res 1995;704:240–45
12. Sheehan JP, Palmer PE, Helm GA,Tuttle JB. MPP+ induced apoptotic cell death in SH-SY5Y neuroblastoma cells: An electron microscope study. J Neurosci Res 1997;48:226–37
13. Hartley A, Stone JM, Heron C, Cooper J, Schapira AHV. Complex I inhibitors induce dose-dependent apoptosis in PC12 cells: Relevance to Parkinson's disease. J Neurochem 1994;63:1987–90
14. Desole MS, Sciola L, Delogu MR, Sircana S, Migheli R, Miele E. Role of oxidative stress in the manganese and 1-methyl-4-(2-ethylphenyl)-1,2,3,6-tetrahydropyridine-induced apoptosis in PC12 cells. Neurochem Int 1997;31:169–76
15. Zhao M, Momma S, Delfani K, et al. Evidence for neurogenesis in the adult mammalian substantia nigra. Proc Natl Acad Sci U S A 2003;100: 7925–30
16. Hoglinger GU, Rizk P, Muriel MP, et al. Dopamine depletion impairs precursor cell proliferation in Parkinson disease. Nat Neurosci 2004;7: 726–35
17. Yamada M, Onodera M, Mizuno Y, Mochizuki H. Neurogenesis in olfactory bulb identified by retroviral labeling in normal and 1-methyl-4-phenyl-1,2,3,6-tetrahydropyridine-treated adult mice. Neuroscience 2004; 124:173–81
18. Doetsch F, Petreanu L, Caille I, Garcia-Verdugo JM, Alvarez-Buylla A. EGF converts transit-amplifying neurogenic precursors in the adult brain into multipotent stem cells. Neuron 2002;36:1021–34
19. Doetsch F, Garcia-Verdugo JM, Alvarez-Buylla A. Cellular composition and three-dimensional organization of the subventricular germinal zone in the adult mammalian brain. J Neurosci 1997;17:5046–61
20. Doetsch F, Caille I, Lim DA, Garcia-Verdugo JM, Alvarez-Buylla A. Subventricular zone astrocytes are neural stem cells in the adult mammalian brain. Cell1999;97:703–16
21. Lois C, Alvarez-Buylla A. Long-distance neuronal migration in the adult mammalian brain. Science 1994;264:1145–48
22. Doetsch F, Alvarez-Buylla A. Network of tangential pathways for neuronal migration in adult mammalian brain. Proc Natl Acad Sci U S A 1996;93:14895–900
23. Brunjes PC, Armstrong AM. Apoptosis in the rostral migratory stream of the developing rat. Brain Res Dev Brain Res 1996;92:219–22
24. Levison SW, Rothstein RP, Brazel CY, Young GM, Albrecht PJ. Selective apoptosis within the rat subependymal zone: A plausible mechanism for determining which lineages develop from neural stem cells. Dev Neurosci 2000;22:106–15
25. Bieb lM, Cooper CM, Winkler J, Kuhn HG. Analysis of neurogenesis and programmed cell death reveals a self-renewing capacity in the adult rat brain. Neurosci Lett 2000;291:17–20
26. Levison SW, Rothstein RP, Romanko MJ, Snyder MJ, Meyers RL, Vannucci SJ. Hypoxia/ischemia depletes the rat perinatal subventricular zone of oligodendrocyte progenitors and neural stem cells. Dev Neurosci 2001;23:234–47
27. Cheng ACS, Milhavet O, Wang S, Mattson MP. p38 MAP kinase mediates nitric oxide-induced apoptosis of neural progenitor cells. J Biol Chem 2001;276:43320–27
28. Leonard JR, D'Sa C, Klocke BJ, Roth KA. Neural precursor cell apoptosis and glial tumorigenesis following transplacental ethyl-nitrosourea exposure. Oncogene 2001;20:8281–86
29. Shinohara C, Gobbel GT, Lamborn KR, Tada E, Fike JR. Apoptosis in the subependyma of young adult rats after single and fractionated doses of x-rays. Cancer Res 1997;57:2694–2702
30. Amano T, Inamura T, Wu CM, et al. Effects of single low dose irradiation on subventricular zone cells in juvenile rat brain. Neurol Res 2002;24:809–16
31. Fukuda H, Fukuda A, Zhu C, et al. Irradiation-induced progenitor cell death in the developing brain is resistant to erythropoietin treatment and caspase inhibition. Cell Death Differ 2004;11:1166–78
32. Taupin P. Consideration of adult neurogenesis from basic science to therapy. Med Sci Monit 2005;11:LE16–17
33. Franklin KBJ, Paxinos GT. The Mouse Brain in Stereotaxic Coordinates. London: Academic Press, 1996
34. Capela A, Temple S. LeX/ssea-1 is expressed by adult mouse CNS stem cells, identifying them as nonependymal. Neuron 2002;35:865–75
35. Simic G, Seso-Simic D, Lucassen PJ, et al. Ultrastructural analysis and TUNEL demonstrate motor neuron apoptosis in Werdnig-Hoffmann disease. J Neuropathol Exp Neurol 2000;59:398–407
36. Cohen GM. Caspases: The executioners of apoptosis. Biochem J 1997; 326:1–16
37. Duan WR, Garner DS, Williams SD, Funckes-Shippy CL, Spath IS, Blomme EA. Comparison of immunohistochemistry for activated caspase-3 and cleaved cytokeratin 18 with the TUNEL method for quantification of apoptosis in histological sections of PC-3 subcutaneous xenografts. J Pathol 2003;199:221–28
38. Doetsch F, Verdugo JM, Caille I, Alvarez-Buylla A, Chao MV, Casaccia-Bonnefil P. Lack of the cell-cycle inhibitor p27Kip1 results in selective increase of transit-amplifying cells for adult neurogenesis. J Neurosci 2002;22:2255–64
39. Doetsch F, Garcia-Verdugo JM, Alvarez-Buylla A. Regeneration of a germinal layer in the adult mammalian brain. Proc Natl Acad Sci U S A 1999;96:11619–24
40. Lois C, Garcia-Verdugo JM, Alvarez-Buylla A. Chain migration of neuronal precursors. Science 1996;271:978–81
41. Magavi SS, Leavitt BR, Macklis JD. Induction of neurogenesis in the neocortex of adult mice. Nature 2000;405:951–55
42. Francis N, Farinas I, Brennan C, et al. NT-3, like NGF, is required for survival of sympathetic neurons, but not their precursors. Dev Biol1 999;210:411–27
43. Lowe B, Avila HA, Bloom FR, Gleeson M, Kusser W. Quantitation of gene expression in neural precursors by reverse-transcription polymerase chain reaction using self-quenched, fluorogenic primers. Anal Biochem 2003;315:95–105
44. Luskin MB. Restricted proliferation and migration of postnatally generated neurons derived from the forebrain subventricular zone. Neuron 1993;11:173–89
45. Petreanu L, Alvarez-Buylla A. Maturation and death of adult-born olfactory bulb granule neurons: Role of olfaction. J Neurosci 2002;22:6106–13

BRAIN RESEARCH 1088 (2006) 57–67

available at www.sciencedirect.com

SCIENCE DIRECT

www.elsevier.com/locate/brainres

BRAIN RESEARCH

Research Report

Cell cycle progression is required for nuclear migration of neural progenitor cells

Masaki Ueno, Kei-ichi Katayama, Hirofumi Yamauchi, Hiroyuki Nakayama, Kunio Doi*

Department of Veterinary Pathology, Graduate School of Agricultural and Life Sciences, The University of Tokyo, 1-1-1 Yayoi, Bunkyo-ku, Tokyo 113-8657, Japan

ARTICLE INFO

Article history:
Accepted 3 March 2006
Available online 2 May 2006

Keywords:
Cell cycle arrest
Elevator movement
Interkinetic nuclear migration
Neural progenitor cell
Neuroepithelial cell
Ventricular zone

Abbreviations:
5AzC, 5-azacytidine
BrdU, 5-bromo-2′-deoxyuridine
CP, cyclophosphamide
VZ, ventricular zone

ABSTRACT

In the developing brain, neural progenitor cells in the ventricular zone (VZ) show a typical migration pattern—interkinetic nuclear migration, in which nuclear position within the VZ is correlated with the cell cycle. However, the mechanisms underlying this regulation remain unclear. To clarify whether the cell cycle progression controls nuclear migration of neural progenitor cells, we determined whether chemically induced cell cycle arrest affected nuclear migration patterns in the VZ. Administration of 5-azacytidine (5AzC) or cyclophosphamide (CP) to pregnant mice induced cell cycle arrest in the fetal neural progenitor cells of the telencephalon: 5AzC induced G2/M-phase arrest, and CP induced S-phase arrest. We used 5-bromo-2′-deoxyuridine (BrdU) labeling to determine the position of the cell in the cell cycle and the nuclei within the VZ at the same time. Cells arrested in G2/M-phase stopped migrating in the inner area of the VZ. Cells arrested in S-phase stopped migrating in the outer area. These results indicate that nuclear position within the VZ was correlated with cell cycle phase, even when the cell cycle was disrupted, and that the nuclei of neural progenitor cells can migrate only when their cell cycle is going. Our results suggest that cell cycle regulators might control the machinery of migration through a common regulatory mechanism.

1. Introduction

Neural progenitor cells have two essential characteristics: limited self-renewal and multipotency. In the fetal brain, they proliferate and differentiate into neurons and, later, glial cells (astrocytes and oligodendrocytes) (Rao, 1999; Qian et al., 2000; Temple, 2001).

Migration and translocation are also important processes for correct brain development. Neural progenitor cells first proliferate in the ventricular zone (VZ) to form a pseudostratified epithelium, where they are called neuroepithelial cells in early and radial glia in later development. After mitosis, some of them migrate beyond the VZ, where they differentiate into neurons or glial cells to form the cortex (Fig. 6A; Angevine and Sidman, 1961; Rakic, 1988; Bayer and Altman, 1995; Tamamaki et al., 2001; Noctor et al., 2004; Miyata et al., 2004; Anthony et al., 2004). Certain critical genes, such as *Reelin*, *Cdk5*, *Dcx*, *Lis1*, and *Nudel*, are involved in this migration (for review, see Feng and Walsh, 2001; Gupta et al., 2002).

Proliferating neural progenitor cells also undergo a typical migration pattern within the VZ-interkinetic nuclear migration (or "elevator movement"), in which the positions of nuclei correlate with the cell cycle phases (Sauer, 1935; Sauer and Walker, 1959; Sidman et al., 1959; Fujita, 1962; Yoshida et al.,

* *Corresponding author.* Fax: +81 3 5841 8185.
E-mail address: ms-ueno@umin.ac.jp (M. Ueno).

0006-8993/$ 7 – see front matter © 2006 Elsevier B.V. All rights reserved.
doi:10.1016/j.brainres.2006.03.042

1987; Takahashi et al., 1993; Hayes and Nowakowski, 2000) (Fig. 6A). S-phase nuclei, located in the outer area of the VZ, migrate inward during G2 phase, and mitosis occurs at the ventricular surface. The nuclei then migrate outward during G1 phase and enter S-phase again. Thus, neural progenitor cells seem to be necessary to proliferate in a precise regulation of cell cycle and nuclear migration. However, the mechanisms underlying this regulation remain unclear.

It has been reported that inhibition of nuclear migration in the VZ by an inhibitor of actin polymerization (e.g., cytochalasin B) or disrupting microtubule function do not affect cell cycle progression because neural progenitor cells which migration are disrupted undergo ectopic mitoses across the width of the VZ (Karfunkel, 1972; Messier and Auclair, 1974; Messier, 1978; Webster and Langman, 1978; Murciano et al., 2002; Gambello et al., 2003). On the other hand, treatments of colchicine or vincristine, a drug known to inhibit mitosis, induce mitotic arrest which are seen preferentially along the ventricular surface (Kallen, 1961, 1962; Langman et al., 1966). These results suggest that the molecules that regulate migration do not control cell cycle progression, but cell cycle regulators might control nuclear migration. However, there is no clear evidence that cell cycle progression in each phase regulates the position of nuclei. In the present study, to clarify whether the regulators of cell cycle control nuclear migration of neural progenitor cells, we induced cell cycle arrest in neural progenitor cells, using two chemicals, 5-azacytidine (5AzC) and cyclophosphamide (CP), and then examined whether the nuclear migration was stopped or not following the cell cycle arrest. Both of these chemicals are anti-cancer drugs, and are known to induce cell cycle arrest followed by apoptosis when administered to fetal brains (Torchinsky et al., 1999; Ueno et al., 2002, 2006; Heringova et al., 2003).

We show here that the nuclear position of neural progenitor cells in the VZ correlates closely with cell cycle phases, even when the cell cycle is disrupted, and that the nuclei of neural progenitor cells can migrate only when their cell cycle is going. These results suggest that the regulation of cell cycle might control migration through common mechanisms.

2. Results

2.1. *Histopathological changes*

Pregnant mice on day 12 of gestation were injected with 5AzC or CP, and we first determined whether 5AzC and CP treatment induced histopathological changes in the VZ of dorsal telencephalic wall.

At 3 to 6 h after 5AzC treatment, more mitotic cells were present along the ventricle than in controls (Figs. 1Aa–c, Ba, b, D), indicating that cell cycle arrest occurred in M phase. Mitotic cells were positive for phospho-Histone H3, a marker for mitotic cells (Figs. 1Ba, b). These cells gradually decreased in number after 6 h, and the number of pyknotic cells among the neural progenitor cells increased between 6 and 12 h (Figs. 1Ac–e, Ca, b, E). These pyknotic cells were positive for terminal deoxynucleotidyltransferase (TdT)-mediated dUTP–biotin nick end labeling (TUNEL) staining, a marker for apoptotic cells (Fig. 1Cb).

In the CP-treated brain, the number of mitotic cells along the ventricle decreased between 6 and 12 h (Figs. 1Ag–i, Ba, c, D), indicating that cell cycle arrest occurred before mitosis. Further, CP treatment increased the number of apoptotic cells, defined as positive for TUNEL staining (Figs. 1Ag–i, Cc, E).

Although apoptosis was induced in the VZ, we can verify that pseudostratified structure remained intact by treatment of these agents (Fig. 1A). It allowed us to evaluate the migration of progenitor cells under the condition that induces cell cycle arrest but do not affect the cell polarity which may be important for migration.

2.2. *Cell cycle analysis*

We next used flow cytometry with propidium iodide (PI) staining, which can bind the DNA and detect the DNA content of the cells, to evaluate the alterations in cell cycle kinetics induced by chemical treatment. The cells were obtained from the fetal telencephalon at embryonic day (E) 12. In E12 to E13 mice, about 70% of cells in the fetal telencephalon are neural progenitor cells (D'Sa-Eipper and Roth, 2000), suggesting that the cells we analyzed were primarily neural progenitor cells.

In the 5AzC-treated group, the number of cells in G2/M phase gradually increased from 3 to 9 h after treatment (control, 5.6 ± 0.1%; 3 h, 8.1 ± 0.8%; 6 h, 17.3 ± 1.2%; 9 h, 20.2 ± 0.5%), and that in S-phase also increased a little, whereas the number in G0/G1 phase decreased (Figs. 2c–e), suggesting that 5AzC induced both S and G2/M arrest. In addition, the number of G2/M-phase cells increased at 9 h more than that at 6 h (6 h, 17.3 ± 1.2%; 9 h, 20.2 ± 0.5%), whereas the number of mitotic cells decreased (Fig. 1D), indicating that 5AzC first induced M arrest at 6 h and then G2 arrest at 9 h. At 12 h, although the number of cells in G2/M remained high (19.0 ± 1.9%), the proportion in S-phase began to decrease, and apoptotic cells in the sub-G1 area increased (8.2 ± 1.5%) (Fig. 2f).

In the CP-treated group, the cell cycle distribution at 3 h did not differ markedly from the control (Fig. 2g). From 6 to 12 h, the number of cells in S-phase increased remarkably (control, 10.0 ± 1.8%; 6 h, 18.6 ± 3.3%; 9 h, 26.2 ± 1.7%; 12 h, 29.7 ± 1.8%), and those in G2/M phase decreased (Figs. 2h–j), suggesting that S-phase arrest occurred. As observed in 5AzC treatment, the number of apoptotic cells in the sub-G1 area also increased after 9 h (8.5 ± 1.5%) (Fig. 2i).

2.3. *Detection of BrdU-positive cells in the cell cycle*

To measure cell cycle and nuclear migration at the same time points, we evaluated the cell cycle transition of BrdU-incorporated cells by using flow cytometry.

The injection protocol is represented in Fig. 3. For the control group, pregnant mice were injected only with BrdU (20 mg/kg), and the fetuses were collected at 1, 3, 6, 9, or 12 h after treatment. Cells from the fetal telencephalon were stained with anti-BrdU antibody and PI and analyzed by flow cytometry. In the BrdU-only control group, BrdU first was incorporated into S-phase cells at 1 h after treatment (Fig. 4Aa). At 3 h, the BrdU-incorporated cells had transited from S to G2/M phase, and some had entered G0/G1 (Fig. 4Ab). At 6 h, most BrdU-positive cells had left S-phase and were in G2/M or

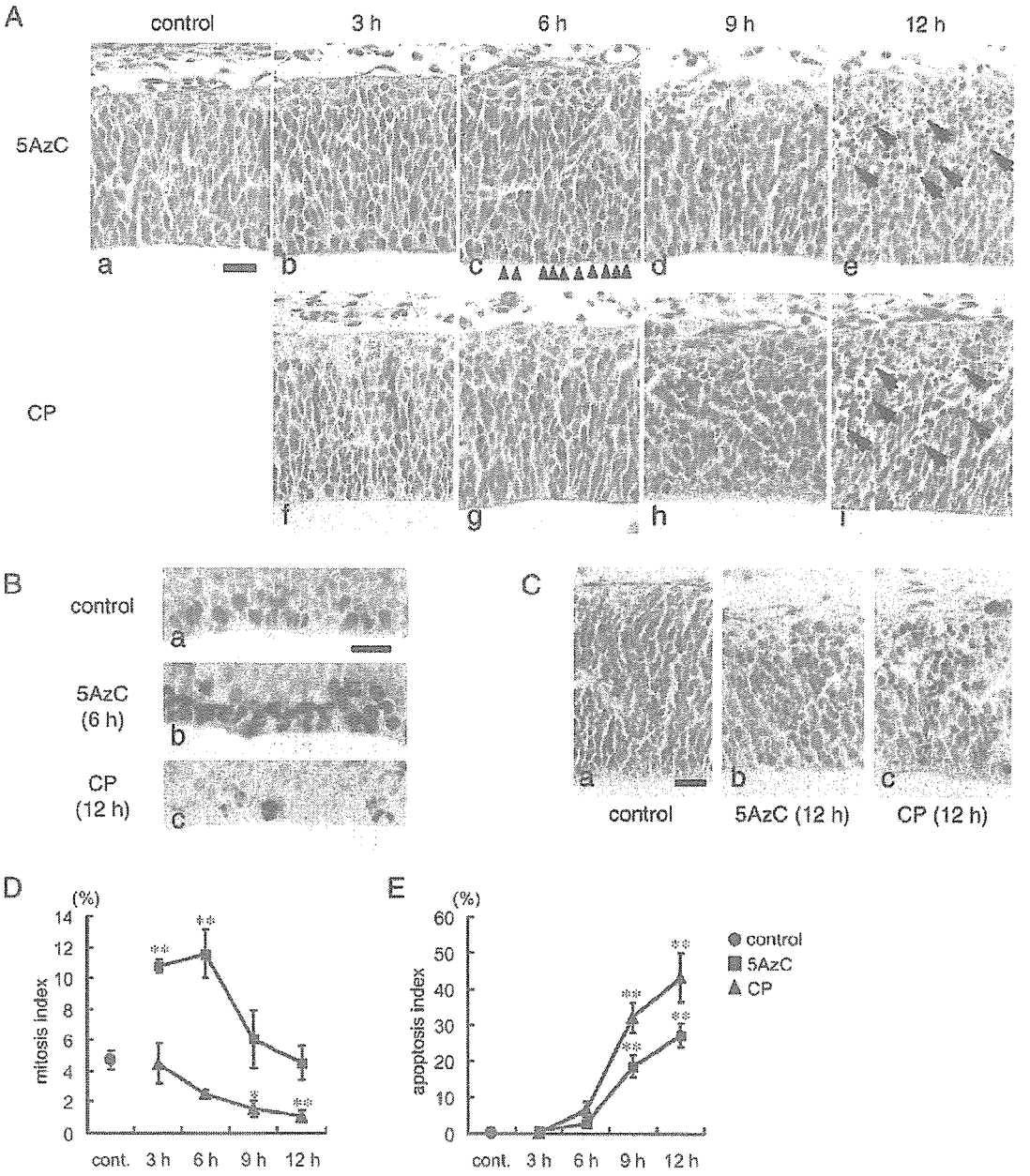

Fig. 1 – Histopathological changes in the VZ of fetal mouse telencephalon. (A) Hematoxylin and eosin staining (a: control [12 h]; b–e: 5AzC-treated; f–i: CP-treated; b, f: 3 h; c, g: 6 h; d, h: 9 h; e, i: 12 h). Arrowheads in panel c: accumulation of mitotic cells along the ventricle. Arrows in panels e and i: apoptotic cells. Scale bar: 50 μm. (B) Staining of phospho-histone H3, a mitotic marker, along the ventricular surface of the VZ (a: control [12 h]; b: 6 h after 5AzC treatment; c: 12 h after CP treatment). Scale bar: 50 μm. (C) TUNEL staining for apoptotic cells (a: control [12 h]; b: 12 h after 5AzC treatment; c: 12 h after CP treatment). Scale bar: 50 μm. (D) The mitosis index (%) of neural progenitor cells at the ventricular surface. (E) The apoptosis index (%) of neural progenitor cells in the VZ. Circle: control (12 h); square: 5AzC; triangle: CP. The indices (%; number of mitotic or apoptotic cells/500 cells in the VZ) are represented as mean ± SD ($n = 3$). $^{*}P < 0.05$, $^{**}P < 0.01$; significantly different from the control (12 h) (ANOVA with Tukey-Kramer test).

G0/G1 phase (Fig. 4Ac). BrdU-positive cells started re-entering S-phase at 9 h (Fig. 4Ad), and most cells completed S-phase reentry by 12 h (Fig. 4Ae). Thus, the duration of a single complete cell cycle is about 9 to 12 h, an assumption that is supported by the report of Takahashi et al. (1995).

In the 5AzC-treated group, 5AzC (10 mg/kg) and BrdU (20 mg/kg) were administered at the same time, and fetuses were collected at 1, 3, 6, 9, or 12 h after treatment (Fig. 3). 5AzC and BrdU are both analogues of nucleic acids and are incorporated simultaneously into DNA during S-phase.

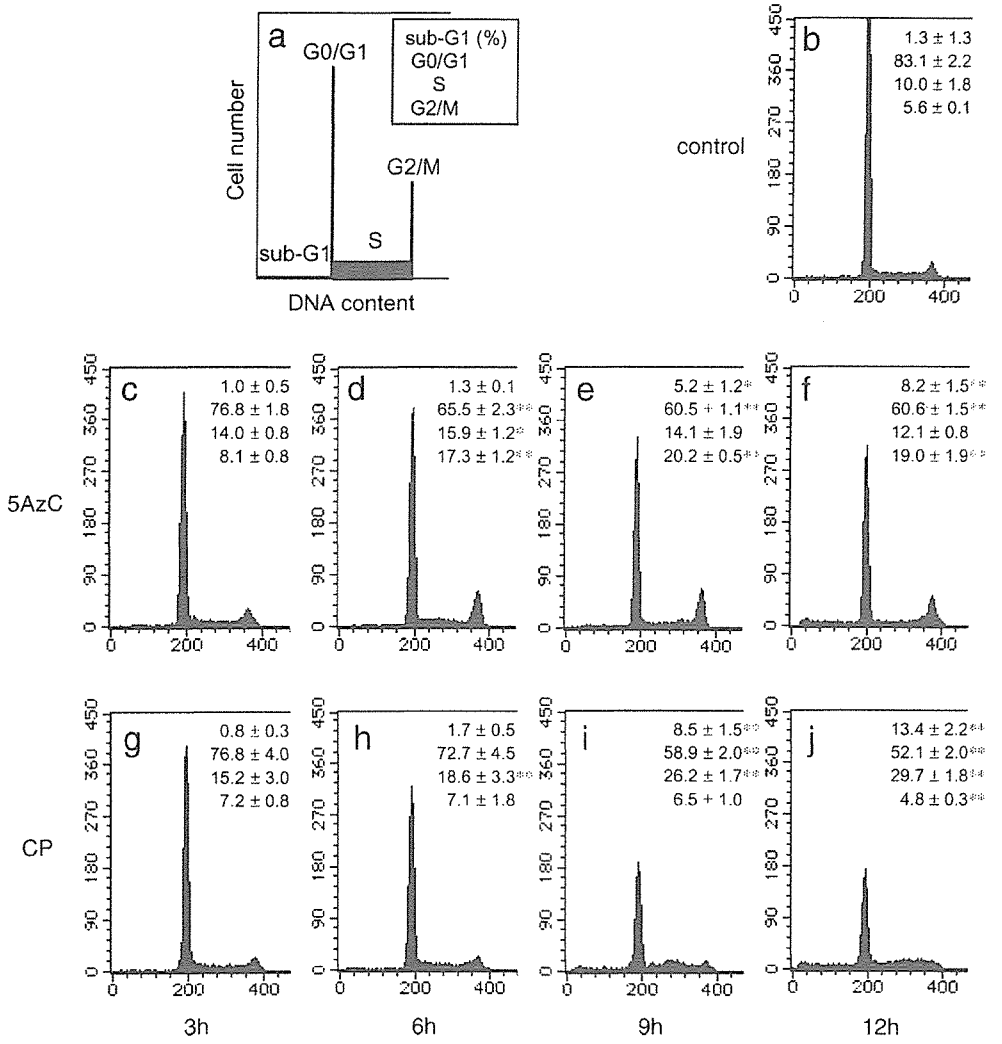

Fig. 2 – Cell cycle analysis of fetal telencephalic cells. (a) Schematic figure of cell cycle analysis. X axis shows PI intensity which is corresponded to DNA content (2n: G0/G1 phase, 4n: G2/M, 2n< and <4n: S, <2n: sub-G1), and Y axis represents cell number. (b) Control (12 h); (c–f) 5AzC-treated; (g–j) CP-treated. (c, g) 3 h; (d, h) 6 h; (e, i) 9 h; (f, j) 12 h after chemical treatment. Percentages for each cell cycle phase are presented as the mean ± SD of 3 dams. *$P < 0.05$, **$P < 0.01$; significantly different from the control group (ANOVA with Tukey-Kramer test). The treatment of 5AzC increased the number of G2/M-phase cells from 3 to 12 h. The treatment of CP increased the number of S-phase cells from 6 to 12 h. Both chemicals induced apoptosis observed in the sub-G1 area from 9 to 12 h.

5AzC treatment allowed BrdU-incorporated positive cells to transit from S to G2/M phase by 6 h, whereas only a few cells moved to G0/G1 phase (Fig. 4Af–h). In contrast to control cells, most of the 5AzC-treated cells remained in G2/M phase from 6 to 9 h after treatment (Figs. 4Ah, i, B: control (6 h), 19.4 ± 5.6%; 5AzC (6 h), 74.9 ± 5.6%, control (9 h), 3.9 ± 2.4%; 5AzC (9 h), 68.4 ± 1.0%). At 12 h, although many BrdU-positive cells were in G2/M phase (Figs. 4Aj, 4B: 34.5 ± 13.3%), some of them moved to G0/G1 phase (17.0 ± 0.6%) or the sub-G1 area and died (13.5 ± 4.5%) (Fig. 4Aj). Thus, 5AzC-treated neural progenitor cells underwent G2/M arrest.

In the CP-treated group, BrdU (20 mg/kg) was administered 6 h after CP treatment (30 mg/kg) (Fig. 3), the time point when S-phase arrest started (Fig. 2h). BrdU was first incorporated into S-phase cells at 1 h after BrdU treatment (Fig. 4Ak). At 3 h, most BrdU-positive cells remained in S-phase, although their DNA content gradually increased (Figs. 4Al, 4B: control (3 h), 33.9 ± 3.7%; CP (3 h), 73.6 ± 3.7%). At 6 h, some of them entered G2/M phase, but many of them were still in S-phase (Figs. 4Am, 4B: control (6 h), 4.9 ± 2.1%; CP (6 h), 63.2 ± 10.3%). These results suggest that CP-treated neural progenitor cells underwent S-phase arrest (or S-phase accumulation).

2.4. *Migration of neural progenitor cell nuclei*

We then examined the distribution of BrdU-positive cells in the VZ of dorsal telencephalic wall by using immunohistochemical staining to determine whether drug treatment induced changes in nuclear migration patterns.

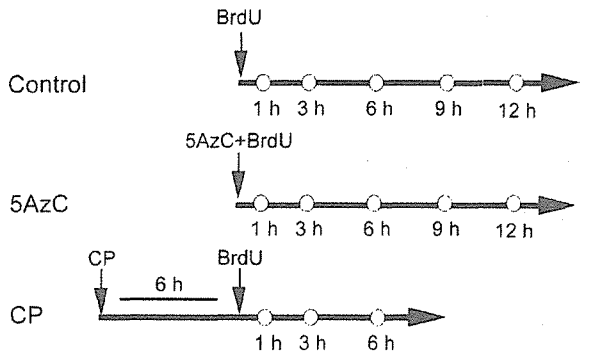

Fig. 3 – Experimental protocols for BrdU incorporation. Control (BrdU, 20 mg/kg), 5AzC-treated group (5AzC, 10 mg/kg, +BrdU), and CP-treated group (CP, 30 mg/kg, +BrdU). White circles represent the time points when the fetuses were collected for either flow cytometry or immunohistochemistry.

In the control group, BrdU-positive nuclei were first observed in the outer area of the VZ, where S-phase cells accumulate (Fig. 5Aa). BrdU-positive nuclei migrated inward and were detected in the mitotic cells at the ventricular surface at 3 h (Fig. 5Ab). At 6 h, most BrdU-positive nuclei were observed in the inner area, while few positive nuclei were observed in the outer area (Fig. 5Ac). The positive nuclei in the inner area correspond to both G2-phase nuclei migrating inward and G1-phase nuclei migrating outward (see Fig. 4Ac). At 9 h, BrdU-positive nuclei were present in the middle of the VZ (Fig. 5Ad) and returned to the outer area at 12 h (Fig. 5Ae). These nuclei correspond to the cells transitioning from G1 to S-phase (Figs. 4Ad, e).

In the 5AzC-treated group, BrdU-positive nuclei were initially observed in the outer area of the VZ, similar to the control group (Fig. 5Af). At 3 h, some BrdU-positive nuclei had moved inward, but many were still present in the outer area (Fig. 5Ag). At 6 h, BrdU-positive nuclei were located in the inner area, and many mitotic cells were BrdU-positive (Fig. 5Ah). At 9 h, BrdU-positive nuclei seemed to stop their translocation in the inner area of the VZ in comparison with the controls (Figs. 5Ad, i, B: control (9 h), 22 ± 5.7%; 5AzC (9 h), 63.2 ± 3.9%), although some cells may have migrated outward after mitosis. Since flow cytometry showed that cells were in G2/M phase at this time point (Figs. 4Ah, i), the delay of nuclear migration to the inner area and G2/M arrest occurred simultaneously. At 12 h, some BrdU-positive nuclei were observed in the middle area and seemed to be migrating toward the outer area again (Fig. 5Aj). These cells could potentially correspond to G0/G1-phase cells (Fig. 4Aj). Some BrdU-positive nuclei had nuclear condensation, a characteristic of apoptosis (arrows in Fig. 5Aj).

In the CP-treated group, BrdU-positive nuclei were observed in the middle and outer area of the VZ, at 1 h after BrdU-treatment (Fig. 5Ak). From 3 to 6 h, they remained in the outer area (Figs. 5Al, m, B: control (6 h), 15.6 ± 4.5%; 5AzC (6 h), 40.5 ± 11.2%), and no BrdU-positive mitotic cells were observed. These BrdU-positive cells were mostly in S-phase, with some in G2/M (Figs. 4Al, m), and some BrdU-positive nuclei showed nuclear condensation (arrows in Fig. 5Am). The results show that the cells in S arrest remained in the outer area, suggesting that S-phase arrest and failure to migrate occurred simultaneously.

3. Discussion

Migration is a critical step in brain development. Differentiating neuronal or glial blast cells migrate in a radial or tangential manner to construct brain structures (Marin and Rubenstein, 2001; Gupta et al., 2002). Proliferating neural progenitor cells, known as neuroepithelial cells in early development and radial glia in later development, also have a specific migration system, interkinetic nuclear migration (also called "elevator movement") (Fig. 6A).

The migration of differentiating neural cells has been studied with various approaches but primarily with mutant or knockout mice (Feng and Walsh, 2001; Gupta et al., 2002). A number of genes, including *Reelin*, *Dab1*, and *Cdk5/p35/p39*, play a role in the signal transduction through the plasma membrane (Ohshima and Mikoshiba, 2002). Other genes, including *DCX*, *LIS1*, and *NUDEL*, are thought to directly regulate the cytoskeleton and mediate cell movement (Feng and Walsh, 2001). The interaction of these two categories of genes is a subject of intense investigation.

On the other hand, the regulation of the nuclear migration of neural progenitor cells is poorly understood. The "elevator movement" exhibited by these nuclei is thought to be dependent on cell cycle progression (Fig. 6A). Indeed, most S-phase nuclei are observed in the outer area of VZ which is shown by ^{3}H-thymidine or BrdU labeling, whereas most mitotic cells are on the ventricular surface (Sauer, 1935; Sauer and Walker, 1959; Sidman et al., 1959; Fujita, 1960, 1962; Yoshida et al., 1987; Takahashi et al., 1992, 1993; Hayes and Nowakowski, 2000). The nuclear migration of neural progenitor cells was confirmed not only by ^{3}H-thymidine and BrdU labeling, but also by time-lapse observations of fluorescently labeled cells (Chenn and McConnell, 1995; Noctor et al., 2001; Miyata et al., 2001). Although S-phase-nuclei and mitosis are located in a restricted region in the VZ under normal circumstances, however, there is no direct evidence that cell cycle progression in each phase regulates the position of nuclei.

In the present study, we examined whether this nuclear migration pattern correlated with cell cycle progression, even when cell cycle progression was chemically disrupted. We used the same marker, BrdU, to examine the cell cycle distribution and morphological distribution of cells in the VZ by coupling immunohistochemical and flow cytometric methods, which is a new method to detect cell cycle progression and nuclear migration simultaneously. As expected, neural progenitor cells stopped their migration according to their phase of cell cycle arrest. 5AzC treatment induced G2/M arrest, and the nuclei of neural progenitor cells stopped their migration in the inner area of the VZ, where they would normally be located during the G2 phase (Fig. 6B). CP treatment induced S-phase arrest, and the nuclei of neural

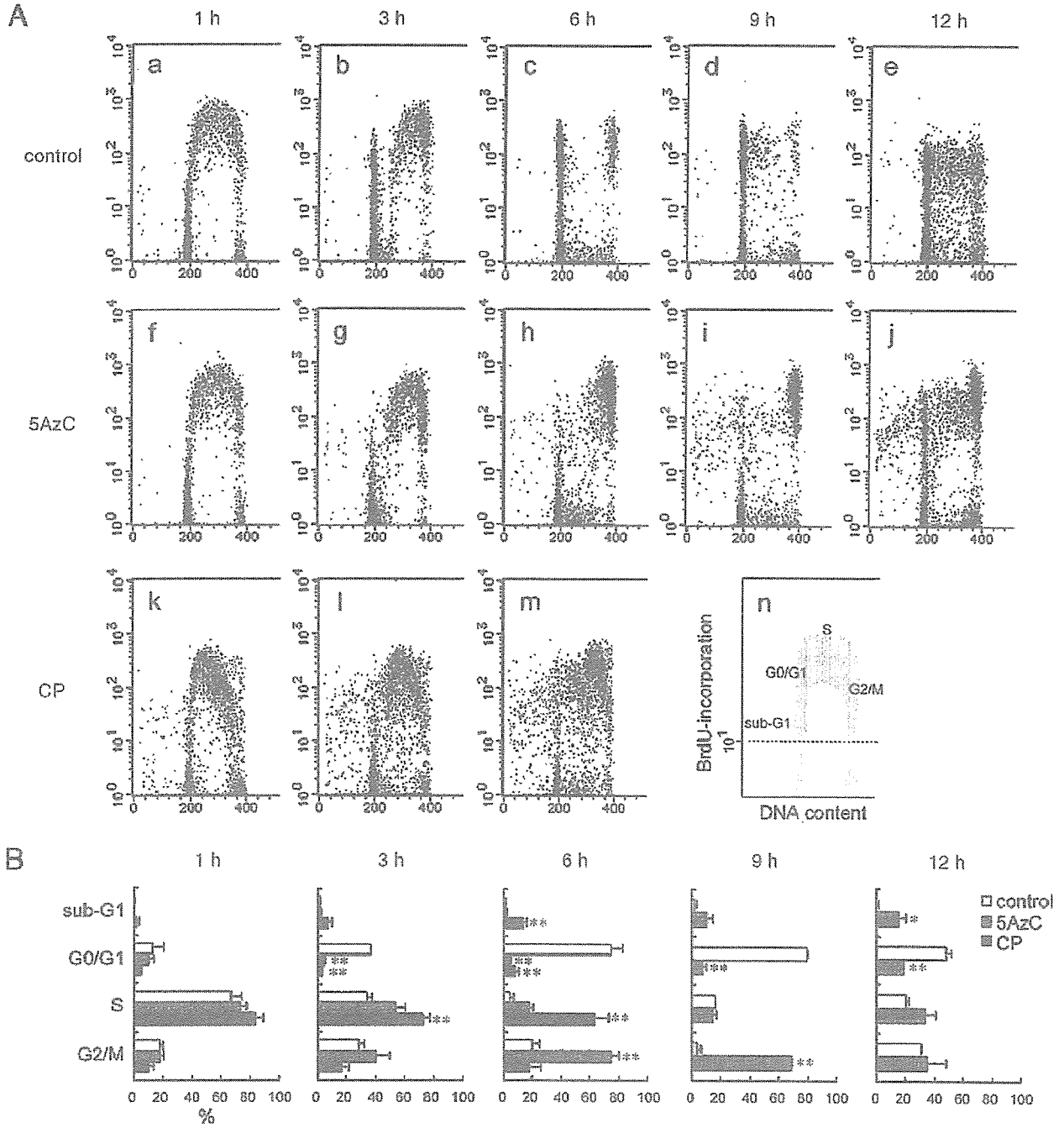

Fig. 4 – Transition of BrdU-incorporated cells in the cell cycle. (A) Detection of BrdU-positive cells in the cell cycle. n: schematic figure of this cell cycle analysis. *X* axis shows PI intensity which is corresponded to DNA content (2n: G0/G1 phase, 4n: G2/M, 2n< and <4n: S, <2n: sub-G1) and *Y* axis represents FITC intensity which is corresponded to BrdU incorporation. The cells that have FITC intensity above the dotted line are BrdU-positive cells. (a–e) Control (BrdU-treated); (f–j) 5AzC and BrdU-treated; (k–m) CP and BrdU-treated. (a, f, k) 1 h; (b, g, l) 3 h; (c, h, m) 6 h; (d, i) 9 h; (e, j) 12 h after BrdU treatment. (B) Distribution of BrdU-positive cells in the cell cycle. White bar: control group, gray bar: 5AzC-treated group, black bar: CP-treated group. Percentages for each cell cycle phase are presented as the mean ± SD of 2 dams. $^{*}P < 0.05$, $^{**}P < 0.01$; significantly different from the control group (ANOVA with Tukey-Kramer test). 5AzC and CP-treated cells delayed in their transition in G2/M and S-phase respectively.

progenitor cells stopped their migration in the outer area of the VZ, where the nuclei of S-phase cells normally exist (Fig. 6C). These results are supported by the report that S-phase arrest induced by ethylnitrosourea also inhibits the nuclear migration of neural progenitor cells (Katayama et al., 2005). It is also reported that chemically induced mitotic arrest to the

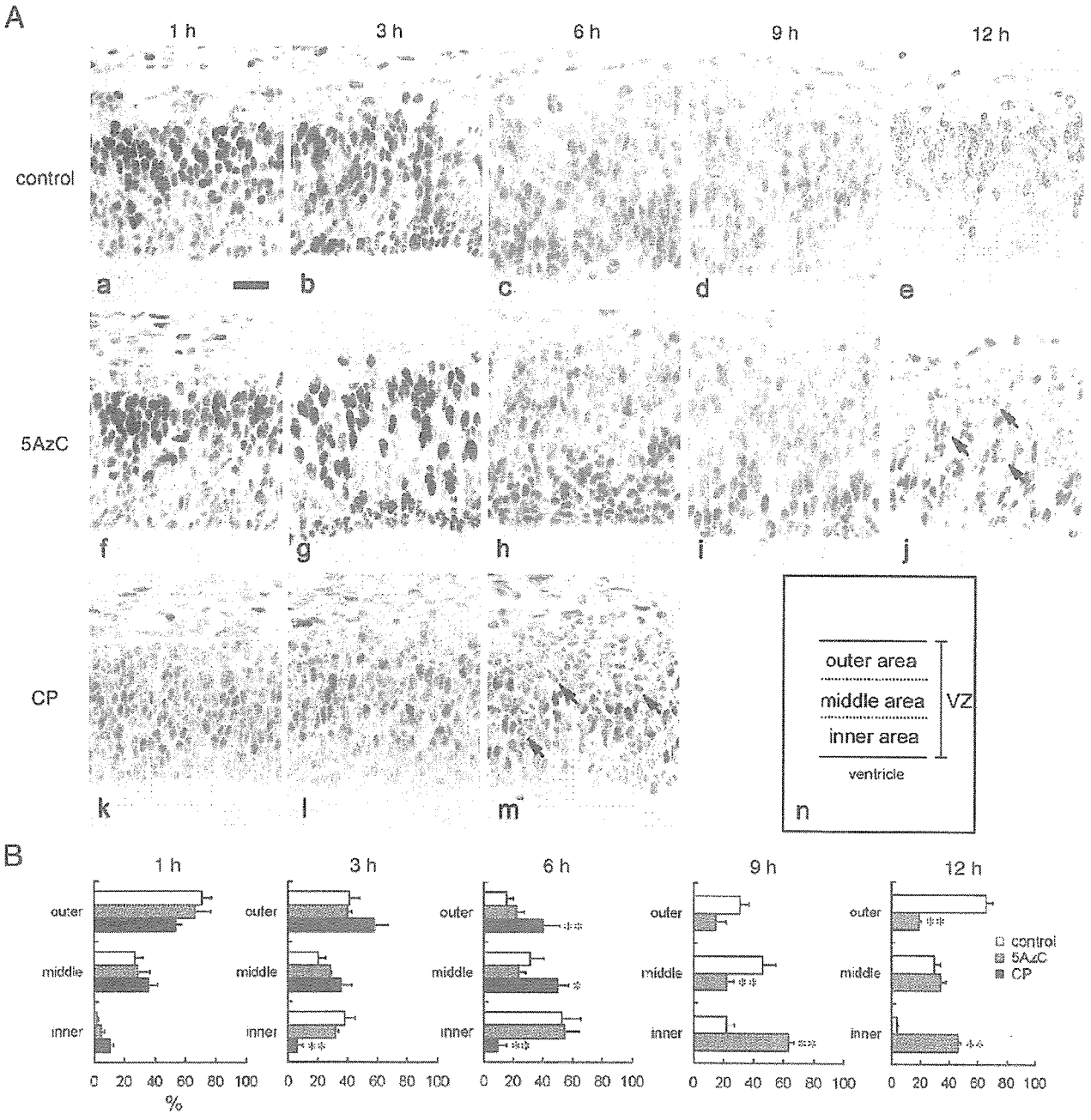

Fig. 5 – Migration of BrdU-positive nuclei of neural progenitor cells in the VZ. BrdU, 5AzC, and CP were administered as shown in Fig. 3. (A) Migration of BrdU-positive nuclei was detected immunohistochemically. Sections of control (a–e), 5AzC-treated (f–j), and CP-treated (k–m) fetuses were stained with anti-BrdU at 1 h (a, f, k), 3 h (b, g, l), 6 h (c, h, m; arrows: apoptotic cells), 9 h (d, i), or 12 h (e, j; arrows: apoptotic cells) after BrdU treatment. For evaluating the migration of BrdU-positive nuclei, the VZ were divided into 3 areas, outer, middle, and inner (n). (B) BrdU-positive nuclei in each area of the VZ were counted, and the percentage per total BrdU-positive nuclei is represented. Each value represents mean ± SD of 2 dams. $^{*}P < 0.05$, $^{**}P < 0.01$; significantly different from the control group (ANOVA with Tukey-Kramer test).

neural progenitor cells stops their migration at the ventricular surface (Kallen, 1961, 1962; Langman et al., 1966). Although we did not investigate other phase arrests (i.e., G1 phase), we propose that the same relationship exists between migration and cell cycle at all phases. Murciano et al. (2002) reported that S-phase arrest by hydroxyurea (HU) do not affect the nuclear migration in the chick diencephalon, suggesting that cell cycle and migration are regulated in a different machinery (for review, see Götz and Huttner, 2005). Although their experimental condition has several unclear points (i.e., degree of S-

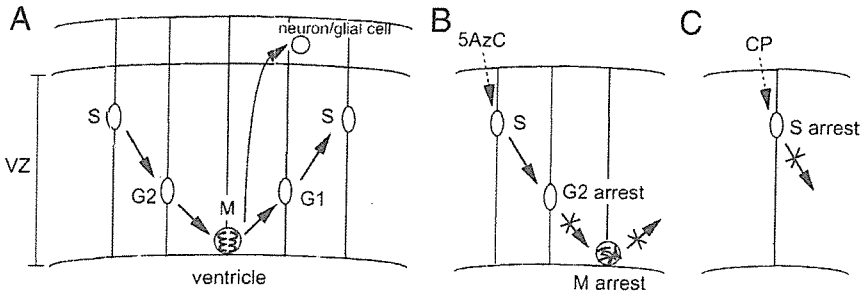

Fig. 6 – Schematic representation of the relationship between chemically induced cell cycle arrest and nuclear migration of neural progenitor cells. (A) Normal interkinetic nuclear migration (elevator movement) of neural progenitor cells. Neural progenitor cells proliferate with their nuclei migrating up and down in the VZ. The progression of this nuclear migration correlates with the phases of the cell cycle. After mitosis, some cells leave the VZ and differentiate into neurons or glial cells. (B) 5AzC induced G2 and M arrest, and the arrest stopped the inward migration of the nuclei. C: CP induced S arrest, which stopped the migration in the outer area of the VZ.

phase arrest, sequential pattern of migration, damage of pseudostratified structure), we have to evaluate the effect of HU using our experimental model to clarify these controversial results.

Our results suggest the presence of a mechanism to connect nuclear migration and cell cycle progression. In addition, inhibition of nuclear migration does not affect cell cycle progression (Karfunkel, 1972; Messier and Auclair, 1974; Messier, 1978; Webster and Langman, 1978; Murciano et al., 2002; Gambello et al., 2003), suggesting that cell cycle regulators control the migration, but migration system does not control cell cycle. It is assumed that, for example, cell cycle regulators that play a role in the G2 transition might also induce inward nuclear migration. Once the cell cycle regulators stop the G2 transition, they also might stop the inward translocation. The same phenomena are assumed to occur in other cell cycle phases.

Recently, Pearson et al. (2005) reported that Ca^{2+} transient precedes the inward nuclear migration in the chick retinal progenitor cells, and gap-junctional communication and hemichannels which regulate propagation of Ca^{2+} increase in neural progenitor cells (Weissman et al., 2004) are necessary for nuclear movement at normal speed. Interestingly, calcium increase is involved in cell cycle progression in radial glial cells (Owens and Kriegstein, 1998; Weissman et al., 2004), and blockade of gap junction or connexin channels suppresses proliferation of neural progenitor cells (Bittman et al., 1997; Goto et al., 2002; Becker and Mobbs, 1999; Cheng et al., 2004). Taken together, it is suggested that blockade of Ca^{2+} increase, gap-junctional communication, or hemichannels may suppress cell cycle progression and then result in inhibition of nuclear migration, which is consistent with our previous model. It would be therefore interesting to examine the relationship among cell cycle regulators, Ca^{2+} modulation, and nuclear migration.

Interkinetic nuclear migration is a very fundamental histogenetic strategy widely used in many epithelial systems including neuroepithelium (Sauer, 1936; Fujita, 1960; Bort et al., 2006), however, biological significance of this migration remains unclear. It is suggested that, in the developing nervous system, this migration is necessary to segregate the VZ into two regions, the apical zone (inner area) and the basal zone (outer area), to keep neurogenesis and DNA replication respectively (Murciano et al., 2002). Thus, this migration seems to be important for completing the brain development in which neurons and glial cells have to be produced in a large number and at an appropriate timing. It is therefore further needed to investigate the molecular mechanism of this typical migration. In this case, our present experimental model will contribute to clarify the mechanism of interkinetic nuclear migration in the developing brain.

4. Experimental procedure

All procedures were approved by the Animal Care and Use Committee of the Graduate School of Agricultural and Life Sciences, The University of Tokyo.

4.1. *Animals*

Timed pregnant C57BL/6J mice were obtained from Japan CLEA (Tokyo, Japan).

4.2. *Chemicals*

5AzC, CP, and BrdU were obtained from Sigma (St. Louis, MO).

4.3. *Chemical treatment for histopathological examination and cell cycle analysis*

On day 12 of gestation, pregnant mice were injected intraperitoneally (i.p.) with 10 mg/kg of 5AzC or 30 mg/kg of CP and then euthanized at 3, 6, 9, or 12 h after treatment. As controls, pregnant mice were injected with an equivalent volume of saline and euthanized at 6 and 12 h after treatment. Collected fetuses were used for histopathological examination and cell cycle analysis.

4.4. *Histopathological examination, immunohistochemistry, and TUNEL staining*

Collected fetuses were fixed in 10% neutral-buffered formalin and embedded in paraffin. Paraffin sections (thickness, 4 μm) were stained with hematoxylin and eosin for histopathological examination.

Some of the sections underwent immunohistochemical staining for phospho-histone H3 by the LSAB method with streptavidin (Dako, Carpinteria, CA). Rabbit anti-phospho-histone H3 polyclonal antibody (Cell Signaling Technology, Beverly, MA) was used as the primary antibody and biotin-labeled goat anti-rabbit IgG (Kirkegaard and Perry, Gaitherburg, MD) as the secondary antibody. The positive signals were visualized using a peroxidase-diaminobenzidine reaction, and then the sections were counterstained with methyl green.

Cells with fragmented DNA were detected by TUNEL method by use of an apoptosis detection kit (Apop Tag; Intergen, Purchase, NY). In brief, multiple fragmented DNA-3′-OH ends on the section were labeled with digoxigenin-dUTP in the presence of TdT enzyme. Peroxidase-conjugated anti-digoxigenin antibody was then reacted with the sections. Apoptotic nuclei were visualized using a peroxidase-diaminobenzidine reaction, and then the sections were counterstained with methyl green.

The indices of mitotic or apoptotic cells (%; number/500 cells in the VZ) were represented as the mean ± SD of 3 dams, and statistical analysis was performed by a one-way ANOVA followed by Tukey-Kramer multiple comparison test.

4.5. *Cell cycle analysis*

The telencephalons of two or three fetuses from each dam (3 to 12 h after treatment, and controls) were obtained under stereoscopic microscopy and then combined and resuspended in HBSS at a concentration of 1–2 × 10^6. Cells were centrifuged for 5 min at 1500×*g* at 4°C, and the supernatant was discarded. After being washed in Dulbecco's PBS (dPBS), the cells were fixed in 70% ethanol at 4°C overnight. Cells were then washed in dPBS and incubated with ribonuclease A (RNase A; 250 μg/ml, Sigma) for 40 min at 37°C. Cells were stained with propidium iodide (PI; 50 μg/ml, Sigma) for 30 min on ice. Cell cycle analysis was performed using the FACS Callibur system (Becton Dickinson, Mountain View, CA), and cell cycle distribution was analyzed by using the Cell Quest program (Becton Dickinson). Percentages for each cell cycle phase were presented as the mean ± SD of 3 dams, and statistical analysis was performed by a one-way ANOVA followed by Tukey-Kramer multiple comparison test.

4.6. *BrdU treatment for evaluating cell cycle transition and migration*

The injection protocol is represented in Fig. 3. As controls, pregnant mice (day E12) were injected with 20 mg/kg of BrdU and euthanized at 1, 3, 6, 9, or 12 h after treatment. For the 5AzC-treated group, pregnant mice were injected i.p. with 10 mg/kg of 5AzC and 20 mg/kg of BrdU at the same time and then euthanized at 1, 3, 6, 9, or 12 h after treatment. In the CP-treated group, pregnant mice on day 12 were first injected i.p. with 30 mg/kg of CP and, 6 h later, were injected i.p. with 20 mg/kg of BrdU. They were then euthanized at 1, 3, or 6 h after BrdU treatment. The collected fetuses were subjected to flow cytometric analysis for investigating the transition in the cell cycle or immunohistochemical staining for the evaluation of nuclear migration patterns.

4.7. *Cell cycle staging of BrdU-positive cells by flow cytometry*

Cells isolated from two or three fetal telencephalons were resuspended and then washed and fixed using the method described for cell cycle analysis. After being fixed, the cells were washed with dPBS, resuspended, and then incubated for 30 min at room temperature (RT) in 2 M HCl containing 0.5% Triton X-100. After being neutralized in 0.1 M $Na_2B_4O_7$, the cells were incubated with an FITC-labeled anti-BrdU monoclonal antibody (Pharmingen, San Diego, CA) for 30 min at RT. They then were resuspended in dPBS containing PI (10 μg/ml) for 30 min on ice and were analyzed with the FACS Callibur system and Cell Quest program (Becton Dickinson). Percentages for each cell cycle phase per total BrdU-positive cells were presented as the mean ± SD of 2 dams, and statistical analysis was performed by a one-way ANOVA followed by Tukey-Kramer multiple comparison test.

4.8. *Evaluation of the nuclear migration pattern of BrdU-positive cells*

Collected fetuses were fixed in 10% neutral-buffered formalin and embedded in paraffin. Paraffin sections (thickness, 4 μm) were used for immunohistochemical staining for BrdU with the LSAB method (Ueno et al., 2002). Mouse anti-BrdU monoclonal antibody (1:100; Dako, Carpinteria, CA) and biotinylated goat anti-mouse IgG antibody (1:400; Kirkegaard and Perry, Gaithersburg, MD) were used as the primary and the secondary antibodies, respectively. Stains were visualized using a peroxidase-diaminobenzidine reaction, and then the sections were counterstained with methyl green. BrdU-positive nuclei in each area of the VZ were counted, and the percentage per total BrdU-positive nuclei was represented as the mean ± SD of 2 dams. Statistical analysis was performed by a one-way ANOVA followed by Tukey-Kramer multiple comparison test.

Acknowledgments

This study was financially supported by the Japan Society for the Promotion of Science.

REFERENCES

Angevine, J.B., Sidman, R.L., 1961. Autoradiographic study of cell migration during histogenesis of cerebral cortex in the mouse. Nature 192, 766–768.

Anthony, T.E., Klein, C., Fishell, G., Heintz, N., 2004. Radial glia

serve as neuronal progenitors in all regions of the central nervous system. Neuron 41, 881–890.
Bayer, S.A., Altman, J., 1995. Neurogenesis and neuronal migration, In: Paxinos, G. (Ed.), The Rat Nervous System, 2nd ed. Academic Press, San Diego, pp. 1070–1074.
Becker, D.L., Mobbs, P., 1999. Connexin alpha1 and cell proliferation in the developing chick retina. Exp. Neurol. 156, 326–332.
Bittman, K., Owens, D.F., Kriegstein, A.R., LoTurco, J.J., 1997. Cell coupling and uncoupling in the ventricular zone of developing neocortex. J. Neurosci. 17, 7037–7044.
Bort, R., Signore, M., Tremblay, K., Barbera, J.P., Zaret, K.S., 2006. Hex homeobox gene controls the transition of the endoderm to a pseudostratified, cell emergent epithelium for liver bud development. Dev. Biol. 290, 44–56.
Cheng, A., Tang, H., Chai, J., Zhu, M., Zhang, X., Rao, M., Mattson, M., 2004. Gap junctional communication is required to maintain mouse cortical neural progenitor cells in a proliferative state. Dev. Biol. 272, 203–216.
Chenn, A., McConnell, S.K., 1995. Cleavage orientation and the asymmetric inheritance of Notch1 immunoreactivity in mammalian neurogenesis. Cell 82, 631–641.
D'Sa-Eipper, C., Roth, K.A., 2000. Caspase regulation of neuronal progenitor cell apoptosis. Dev. Neurosci. 22, 116–124.
Feng, Y., Walsh, C.A., 2001. Protein-protein interactions, cytoskeletal regulation and neuronal migration. Nat. Rev., Neurosci. 2, 408–416.
Fujita, S., 1960. Mitotic pattern and histogenesis of the central nervous system. Nature 185, 702–703.
Fujita, S., 1962. Kinetics of cellular proliferation. Exp. Cell Res. 28, 52–60.
Gambello, M.J., Darling, D.L., Yingling, J., Tanaka, T., Gleeson, J.G., Wynshaw-Boris, A., 2003. Multiple dose-dependent effects of Lis1 on cerebral cortical development. J. Neurosci. 23, 1719–1729.
Gupta, A., Tsai, L.H., Wynshaw-Boris, A., 2002. Life is a journey: a genetic look at neocortical development. Nat. Rev., Genet. 3, 342–355.
Goto, T., Takahashi, T., Miyama, S., Nowakowski, R.S., Bhide, P.G., Caviness Jr., V.S., 2002. Developmental regulation of the effects of fibroblast growth factor-2 and 1-octanol on neurogenesis: implications for a hypothesis relating to mitogen-antimitogen opposition. J. Neurosci. Res. 69, 714–722.
Götz, M., Huttner, W.B., 2005. The cell biology of neurogenesis. Nat. Rev., Mol. Cell Biol. 6, 777–788.
Hayes, N.L., Nowakowski, R.S., 2000. Exploiting the dynamics of S-phase tracers in developing brain: interkinetic nuclear migration for cells entering versus leaving the S-phase. Dev. Neurosci. 22, 44–55.
Heringova, L., Jelinek, R., Dostal, M., 2003. Cell-cycle alterations underlie cyclophosphamide-induced teratogenesis in the chick embryo. Birth Defects Res., A Clin. Mol. Teratol. 67, 438–443.
Kallen, B., 1961. Studies on cell proliferation in the brain of chick embryos with special reference to the mesencephalon. Z. Anat. Entwicklungsgesch. 122, 388–401.
Kallen, B., 1962. Mitotic patterning in the central nervous system of chick embryos; studied by a colchicine method. Z. Anat. Entwicklungsgesch. 123, 309–319.
Karfunkel, P., 1972. The activity of microtubules and microfilaments in neurulation in the chick. J. Exp. Zool. 181, 289–301.
Katayama, K., Ueno, M., Yamauchi, H., Nagata, T., Nakayama, H., Doi, K., 2005. Ethylnitrosourea induces neural progenitor cell apoptosis after S-phase accumulation in a p53-dependent manner. Neurobiol. Dis. 18, 218–225.
Langman, J., Guerrant, R.L., Freeman, B.G., 1966. Behavior of neuro-epithelial cells during closure of the neural tube. J. Comp. Neurol. 127, 399–411.
Marin, O., Rubenstein, J.L., 2001. A long, remarkable journey: tangential migration in the telencephalon. Nat. Rev., Neurosci. 2, 780–790.
Messier, P.E., 1978. Microtubules, interkinetic nuclear migration and neurulation. Experientia 34, 289–296.
Messier, P.E., Auclair, C., 1974. Effect of cytochalasin B on interkinetic nuclear migration in the chick embryo. Dev. Biol. 36, 218–223.
Miyata, T., Kawaguchi, A., Okano, H., Ogawa, M., 2001. Asymmetric inheritance of radial glial fibers by cortical neurons. Neuron 31, 727–741.
Miyata, T., Kawaguchi, A., Saito, K., Kawano, M., Muto, T., Ogawa, M., 2004. Asymmetric production of surface-dividing and non-surface-dividing cortical progenitor cells. Development 131, 3133–3145.
Murciano, A., Zamora, J., Lopez-Sanchez, J., Frade, J.M., 2002. Interkinetic nuclear movement may provide spatial clues to the regulation of neurogenesis. Mol. Cell. Neurosci. 21, 285–300.
Noctor, S.C., Flint, A.C., Weissman, T.A., Dammerman, R.S., Kriegstein, A.R., 2001. Neurons derived from radial glial cells establish radial units in neocortex. Nature 409, 714–720.
Noctor, S.C., Martinez-Cerdeno, V., Ivic, L., Kriegstein, A.R., 2004. Cortical neurons arise in symmetric and asymmetric division zones and migrate through specific phases. Nat. Neurosci. 7, 136–144.
Ohshima, T., Mikoshiba, K., 2002. Reelin signaling and Cdk5 in the control of neuronal positioning. Mol. Neurobiol. 26, 153–166.
Owens, D.F., Kriegstein, A.R., 1998. Patterns of intracellular calcium fluctuation in precursor cells of the neocortical ventricular zone. J. Neurosci. 18, 5374–5388.
Pearson, R.A., Luneborg, N.L., Becker, D.L., Mobbs, P., 2005. Gap junctions modulate interkinetic nuclear movement in retinal progenitor cells. J. Neurosci. 25, 10803–10814.
Qian, X., Shen, Q., Goderie, S.K., He, W., Capela, A., Davis, A.A., Temple, S., 2000. Timing of CNS cell generation: a programmed sequence of neuron and glial cell production from isolated murine cortical stem cells. Neuron 28, 69–80.
Rakic, P., 1988. Specification of cerebral cortical areas. Science 241, 170–176.
Rao, M.S., 1999. Multipotent and restricted precursors in the central nervous system. Anat. Rec. 257, 137–148.
Sauer, F.C., 1935. Mitosis in the neural tube. J. Comp. Neurol. 62, 377–405.
Sauer, F.C., 1936. The interkinetic migration of embryonic epithelial nuclei. J. Morphol. 60, 1–11.
Sauer, M.E., Walker, B.E., 1959. Radioautographic study of interkinetic nuclear migration in the neural tube. Proc. Soc. Exp. Biol. Med. 101, 557–560.
Sidman, R.L., Miale, I.L., Feder, N., 1959. Cell proliferation and migration in the primitive ependymal zone: an autoradiographic study of histogenesis in the nervous system. Exp. Neurol. 1, 322–333.
Takahashi, T., Nowakowski, R.S., Caviness Jr., V.S., 1992. BUdR as an S-phase marker for quantitative studies of cytokinetic behaviour in the murine cerebral ventricular zone. J. Neurocytol. 21, 185–197.
Takahashi, T., Nowakowski, R.S., Caviness Jr., V.S., 1993. Cell cycle parameters and patterns of nuclear movement in the neocortical proliferative zone of the fetal mouse. J. Neurosci. 13, 820–833.
Takahashi, T., Nowakowski, R.S., Caviness Jr., V.S., 1995. The cell cycle of the pseudostratified ventricular epithelium of the embryonic murine cerebral wall. J. Neurosci. 15, 6046–6057.
Tamamaki, N., Nakamura, K., Okamoto, K., Kaneko, T., 2001. Radial glia is a progenitor of neocortical neurons in the developing cerebral cortex. Neurosci. Res. 41, 51–60.

Temple, S., 2001. The development of neural stem cells. Nature 414, 112–117.

Torchinsky, A., Ivnitsky, I., Savion, S., Shepshelovich, J., Gorivodsky, M., Fein, A., Carp, H., Schwartz, D., Frankel, J., Rotter, V., Toder, V., 1999. Cellular events and the pattern of p53 protein expression following cyclophosphamide-initiated cell death in various organs of developing embryo. Teratog., Carcinog., Mutagen. 19, 353–367.

Ueno, M., Katayama, K., Nakayama, H., Doi, K., 2002. Mechanisms of 5-azacytidine (5AzC)-induced toxicity in the rat foetal brain. Int. J. Exp. Pathol. 83, 139–150.

Ueno, M., Katayama, K., Yamauchi, H., Nakayama, H., Doi, K., 2006. Cell cycle and cell death regulation of neural progenitor cells in the 5-azacytidine (5AzC)-treated developing fetal brain. Exp. Neurol. 198, 154–166.

Webster, W., Langman, J., 1978. The effect of cytochalasin B on the neuroepithelial cells of the mouse embryo. Am. J. Anat. 152, 209–221.

Weissman, T.A., Riquelme, P.A., Ivic, L., Flint, A.C., Kriegstein, A.R., 2004. Calcium waves propagate through radial glial cells and modulate proliferation in the developing neocortex. Neuron 43, 647–661.

Yoshida, Y., Yamada, M., Wakabayashi, K., Ikuta, F., 1987. Immunohistochemical detection of DNA replicating cells in the developing nervous system: use of bromodeoxyuridine and its monoclonal antibody to rat fetuses. Biomed. Res. 8, 431–444.

Available online at www.sciencedirect.com

ScienceDirect

Neurotoxicology and Teratology 28 (2006) 664–672

NEUROTOXICOLOGY AND TERATOLOGY

www.elsevier.com/locate/neutera

Etoposide induces apoptosis and cell cycle arrest of neuroepithelial cells in a p53-related manner

Chunja Nam *, Hirofumi Yamauchi, Hiroyuki Nakayama, Kunio Doi

Department of Veterinary Pathology, Graduate School of Agricultural and Life Sciences, The University of Tokyo, 1-1-1 Yayoi, Bunkyo-ku, Tokyo 113-8657, Japan

Received 23 March 2006; received in revised form 23 August 2006; accepted 11 September 2006
Available online 27 September 2006

Abstract

We clarified that etoposide (VP-16), a topoisomerase II inhibitor, induced apoptosis in the mouse fetal brain. Apoptotic mechanisms and cell cycle arrest in this system were investigated. Four mg/kg of VP-16 was injected into pregnant mice on day 12 of gestation (GD12). The cell cycle and expression of protein and mRNA of p53 and its transcriptional target genes were examined in the fetal brain. The number of p53- and p21-protein-positive cells peaked at 4 h after treatment (HAT). The expression of *p21* mRNA was significantly increased at 4 HAT and 8 HAT. The expression of *fas* mRNA was significantly increased from 2 to 12 HAT. Significant expression of *puma* mRNA was observed from 1 HAT to 48 HAT. Flow cytometric analysis revealed that VP-16 induced S-phase accumulation and G2 arrest at 4 and 8 HAT, and VP-16-induced apoptosis was significantly increased from 4 to 24 HAT. In an experiment using BrdU treatment of pregnant mice, the migration of neuroepithelial cells in the fetuses was delayed as compared to the migration of controls, and BrdU-positive signals were observed in some pyknotic cells from 8 to 12 HAT. The present results suggest that VP-16 might induce cell cycle arrest at G2/M phase and apoptosis in a p53-related manner.

Keywords: Etoposide; Apoptosis; G2/M arrest; p53; Mouse fetal brain

1. Introduction

VP-16, a topoisomerase II inhibitor, is widely used as a chemotherapic agent for small cell lung cancer, testicular cancers and lymphomas [6,11,37,39]. VP-16 is also known to be a teratogen, and it brings on skeletal malformation and anomalies of the CNS in mice and rats when administrated during early gestational stages [39]. VP-16 interferes with topoisomerase II activity and causes DNA double-stranded breaks through the formation of a cleavage complex containing DNA-drug-enzyme [10]. In our previous study, we showed that the thickness of the cerebral cortex was decreased in the neonates from dams treated with VP-16 on gestation day 12 (GD12) as compared to control neonates (data was not reported). VP-16 immediately induced cell damage and apoptosis in the CNS of mouse fetuses after its administration to pregnant mice on GD12 [28].

The *p53* tumor suppressor protein is activated by DNA damage and other cellular stresses, the induction of cell cycle arrest, DNA repair and apoptosis [20,23,41,43]. In response to genotoxic stress, p53 transactivates its target genes [2,7,12,40]. p53-dependent upregulation of p21 and Gadd45 induces growth arrest [8,17], and it also regulates the repair of DNA damage [24,25,34,36]. p53-dependent apoptosis has been suggested to be mediated by the transactivation of *bax* [38], *fas* [27], *PUMA* (p53-upregulated modulator of apoptosis) [16], *Noxa* [31] and other p53-inducible genes. Cyclin G1 is also a target of p53 [32], and regulates the accumulation and degradation of *p53* protein in association with mdm2 [19].

In this study, we investigated the mechanism of neuroepithelial cell apoptosis in VP-16-exposed mouse fetuses. We examined sequential changes in expression of p53 and its target genes using immunohistochemistry for p53 and p21, and reverse transcription-polymerase chain reaction (RT-PCR) for *p21*, *bax*, *cyclin G1*, *fas*, and *puma*. We also performed cell cycle analysis using flow cytometry, and immunohistochemistry using the 5-bromo-2′-deoxy-uridine (BrdU)-incorporation method to clarify the migration of neuroepithelial cells.

* Corresponding author. Tel./fax: +81 3 5841 5401 8185.
E-mail address: vet0215@yahoo.co.kr (C. Nam).

0892-0362/$ - see front matter © 2006 Elsevier Inc. All rights reserved.
doi:10.1016/j.ntt.2006.09.021

2. Materials and methods

2.1. Animals and chemicals

Eight-week-old pregnant ICR (Crj:CD-1) mice were obtained from Charles River Japan Co., Yokohama, Japan. Mice were kept in an isolator cage (Niki Shoji Co., Tokyo) under controlled conditions (23±2 °C with 55±5% humidity and a 14-h light/10-h dark cycle) and were fed commercial pellets (MF, Oriental Yeast Co., Ltd., Tokyo) and provided with tap water *ad libitum*.

VP-16 (Sigma, St. Louis, MO) was dissolved in 1% dimethyl sulphoxide solution in physiologic saline.

2.2. Experimenal design

In the first experiment, twenty-one 8-week-old pregnant mice (n=3 per time point) were injected with 4 mg/kg of VP-16 intraperitoneally (i.p.) on GD 12. As controls, 21 age-matched pregnant mice (n=3 per time point) were injected i.p. with 1% DMSO solution on GD 12, and three dams were sacrificed by exsanguination under ether anesthesia at 1, 2, 4, 8, 12, 24, and 48 h after treatment (HAT). Telencephalons of six fetuses from each dam were obtained and frozen at −80 °C, and then subjected to RT-PCR analysis. The other fetuses were fixed in 10% neutral-buffered formalin for immunohistochemistry performed as described below.

In the second experiment, exactly the same protocol was used and the telencephalons from six fetuses of each dam were processed for cell cycle analysis as described below.

In the third experiment, 14 8-week-old pregnant mice were simultaneously treated with 4 mg/kg of VP-16 and 20 mg/kg of BrdU i.p. on GD12. As controls, 14 age-matched pregnant mice were injected i.p. with 1% DMSO solution and 20 mg/kg of BrdU on GD12. Two dams of each group were sacrificed by exsanguination under ether anesthesia at 1, 2, 4, 8, 12, 24, and 48 HAT. Fetuses were fixed in 10% neutral-buffered formalin for histopathology and BrdU-immunohistochemistry.

The protocol of the present study was approved by the Laboratory Animal Use and Care Committee of the Graduate School of Agricultural and Life Sciences, the University of Tokyo.

2.3. In situ detection of fragmented DNA (apoptosis)

DNA fragmentation was examined in the paraffin sections by a modified TUNEL (Terminal deoxynucleotidyl Transferase Biotin-dUTP Nick End Labeling) method, which has been widely used for the detection of apoptotic cells. A commercial apoptosis detection kit (ApopTag® Peroxidase *In situ* Apoptosis Detection Kit; Chemicon, CA) was used in the present study. In brief, multiple fragmented DNA 3′-OH ends on a deparaffinized section were labeled with digoxigenin-dUTP in the presence of terminal deoxynucleotidyl transferase (TdT). Peroxidase-conjugated anti-digoxigenin antibody was then reacted with the section. Apoptotic nuclei were visualized by diaminobenzidine (DAB) reaction. The sections were then counterstained with methyl green.

2.4. Immunohistochemistry

Formalin-fixed tissues were embedded in paraffin. For detection of p53, deparaffinized sections were immersed in 10 mM citrate buffer, pH 6.0, and autoclaved at 120 °C for 17 min. Endogenous peroxidase activity was quenched by immersing the sections in 0.3% H_2O_2 in methanol for 30 min, and non-specific reactions were avoided by incubating the sections in 8% skim milk at 37 °C for 40 min. The sections were then reacted with rabbit antibody against p53 (1:300; Santa Cruz) diluted with Tris-buffered saline (TBS) at 4 °C overnight. The sections were further treated with an Envision+ kit (Dako, Carpinteria, CA) at room temperature for 40 min.

For p21-immunostaining, a TSA Biotin System kit (PerkinElmer, Boston, MA) was used. Deparaffinized sections were immersed in 10 mM citrate buffer, pH 6.0, and autoclaved at 120 °C for 20 min. Endogenous peroxidase activity was quenched by immersing the sections in 0.3% H_2O_2 in methanol for 30 min. The sections were incubated with TNB at room temperature for 30 min, and then immediately reacted with mouse antibody against p21 (1:100; PharMingen, San Diego, CA) in TNB at 4 °C overnight. The sections were further incubated with biotinylated antibody against mouse IgG (1:400; Kirkegaard and Perry, Gaitherburg, MD) in TNB for 40 min, with streptoavidin (1:300; Dako) in TNB for 40 min, with biotinyl tyramide amplification reagent at room temperature for 10 min, and finally with SA-HRP in TNB buffer at room temperature for 30 min.

For detection of BrdU, sections were treated with 0.1% trypsin and 0.1% calcium chloride in Tris-buffer at 37 °C and 1 N HCl at room temperature for 30 min, each. Endogenous peroxidase activity was quenched by immersing in 0.3% H_2O_2 in methanol for 30 min. The sections were incubated in 8% skim milk at 37 °C for 40 min to reduce non-specific reactions, and incubated with mouse antibody against BrdU (1:100; Dako) in TBS at 4 °C overnight. The sections were incubated with biotinylated antibody against mouse IgG (1:400; Kirkegaard and Perry) and then with streptoavidin (1:300; Dako) in TBS buffer.

The sections were visualized using the peroxidase–diaminobenzidine reaction and then counterstained with methyl green. Positive cells in the telencephalic wall were counted under a light microscope (×400). p53- or p21-positive surviving neuroepithelial cells in the telencephalic wall were counted in three fetuses randomly chosen from each dam. One thousand cells were counted in each brain. The index of positive cells (%) was expressed as the Mean±standard deviation (S.D.) at each point of examination, and a statistical analysis was done with Student's t test comparing between the control and VP-16-treated groups.

2.5. RNA extraction and RT-PCR analysis

The telencephalons of six fetuses from each dam were pooled and the total cellular RNA was extracted from each homogenized sample using an Isogen kit (Nippon Gene, Toyama, Japan). The RT reaction for synthesizing the first-

Table 1
Primer sequences and cycle number

Gene	Sense primer	Antisense primer	Cycle numbers
p53	GCCAGGAGACATTTTCAGGC	AACTGCACAGGGCACGTCTT	25
p21	AATCCTGGTGATGTCCGACC	GACCAATCTGCGCTTGGAGT	27
fas	GCTCAGAAGGGAAGGAGTAC	ACTGGAGGTTCTAGATTCAGG	32
bax	TTCATCCAGGATCGAGCAGG	TGAGGACTCCAGCCACAAAGAT	25
cyclin G	CTTTGGCTTTGACACGGAGAC	GGAATCGTTGGGAGGTGAGTT	29
puma	ATGGCGGACGACCTCAAC	AGTCCCATGAAGAGATTGTACATGAC	32
GAPDH	TGATGGGTGTGAACCACGAG	TTGAAGTCGCAGGAGACAACC	21

strand cDNA was carried out using an oligo $(dT)_{12-18}$ primer and SUPERSCRIPT™ II Rnase H⁻ Reverse Transcriptase (Gibco, Gaithersburg, MD). PCR was performed using oligonucleotide primers sets corresponding to the cDNA sequences of p53's transcriptional target genes (*p21*, *bax*, *cyclin G*, *fas*, and *puma*), and glyceraldehyde-3-phosphate dehydrogenase (*GAPDH*) (Table 1). PCR amplifications were performed in 100 μl of reaction mixture containing 5 μl of 10×PCR buffer (100 mM Tris–HCl buffer, 500 mM KCl, and 15 mM $MgCl_2$; Takara, Shiga, Japan), 5 μl dNTP (Takara), 1.25 U of Taq™, 50 pM each of sense and antisense primer, and 1 μl of cDNA. After an initial denaturation at 94 °C for 7 min, amplification was performed in a Takara PCR Thermal cycler SP (Takara) (Table 1) under the following conditions: 1 min of denaturation at 94 °C, 1 min of annealing at 50 °C (*fas*), 57 °C (*puma*) or 58.5 °C (others), and 1 min of extension at 72 °C. Amplification of *GAPDH* mRNA was used as the control for template concentration. The PCR products were electrophoretically separated in 2% agarose S (Nippon Gene) in TBE buffer (89 mM Tris-aminomethane, 89 mM boric acid, 10 mM EDTA). The gels were stained with ethidium bromide (Gibco). Fluorescent bands were visualized using a UV-CCD video system

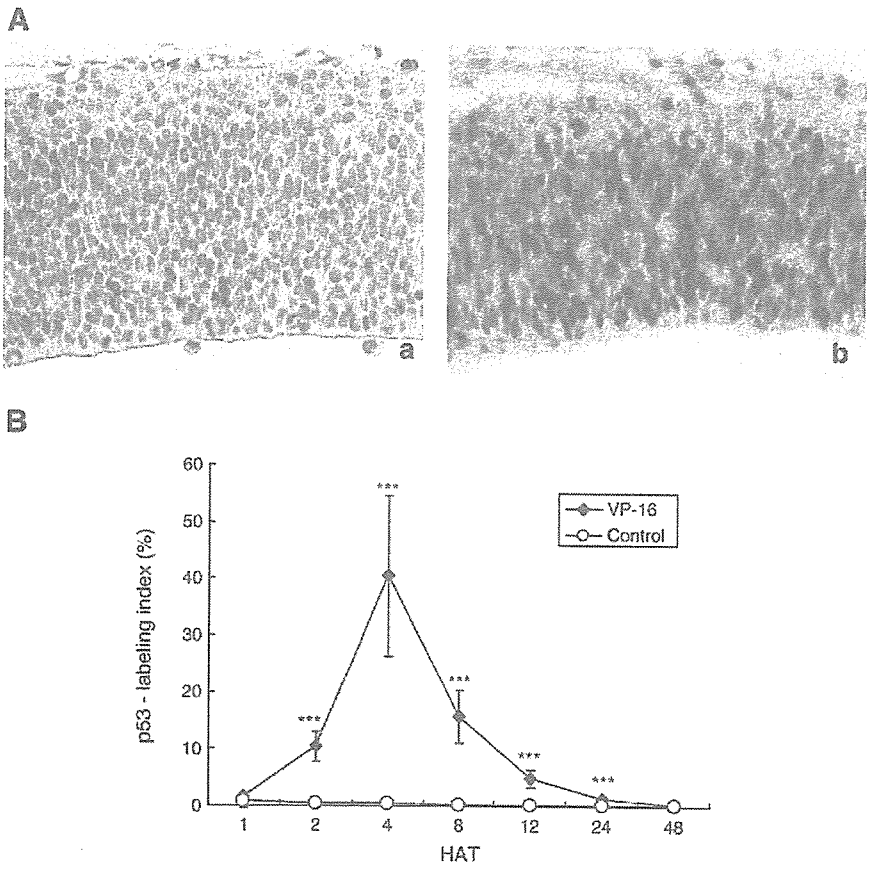

Fig. 1. Immunohistochemistry for p53. (A) p53-positive cells in the fetal brains of the control (a) and VP-16 treated (b) group at 4 HAT. (B) Changes in the p53-labeling index in mouse fetal telencephalon. Each value represents the mean±SD of 3 fetuses from each dam. $^{**}p<0.01$, $^{***}p<0.001$: significantly different from controls by Student's *t* test. ×200.

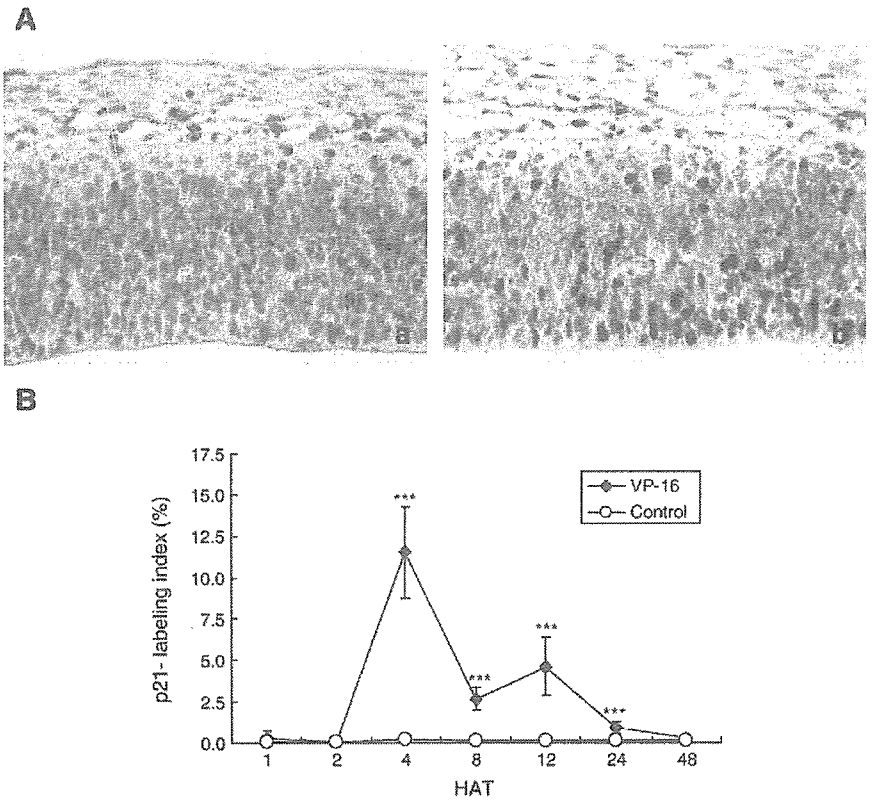

Fig. 2. Immunohistochemistry for p21. (A) p21-positive cells in the fetal brain of the control (a) and VP-16 treated (b) group at 4 HAT. (B) Changes in the p21-labeling index in mouse fetal telencephalon. Each value represents the mean±S.D. of 3 fetuses from each dam. $^{**}p<0.01$, $^{***}p<0.001$: significantly different from controls by Student's t test. ×200.

(EpiLight$_{UVFA1100}$; AISIN COSMOS, Tokyo, Japan) and were analyzed using Quantity One image-analysis software (pdi, NY). The intensity of each band relative to the *GAPDH* band was represented as the mean±S.D. The significance of differences between the control group and HU-treated group was evaluated with Student's t test.

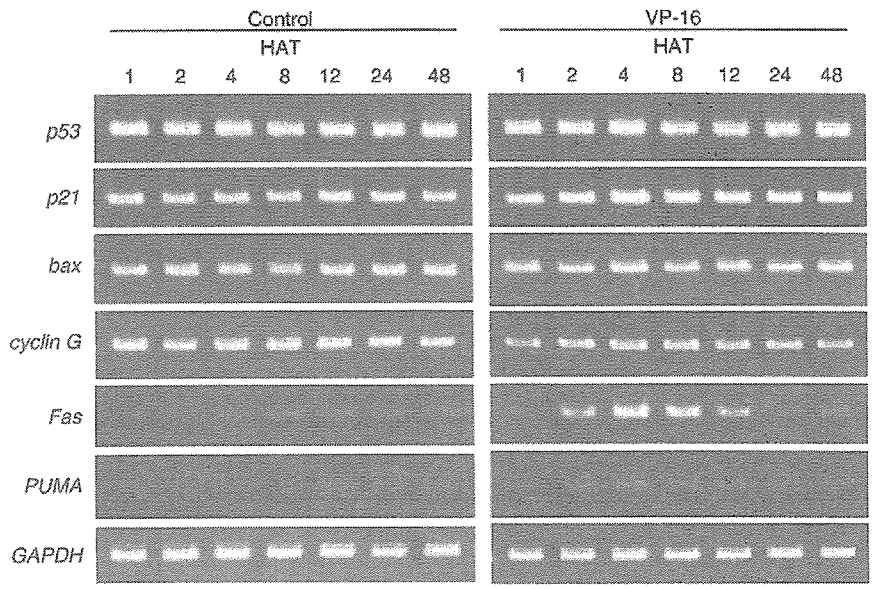

Fig. 3. mRNA expression of p53 and its transcriptional target genes analyzed by RT-PCR. Agarose gel electrophoresis. Expression of a few p53 target genes (*p21*, *fas* and *puma*) was elevated after VP-16 treatment.

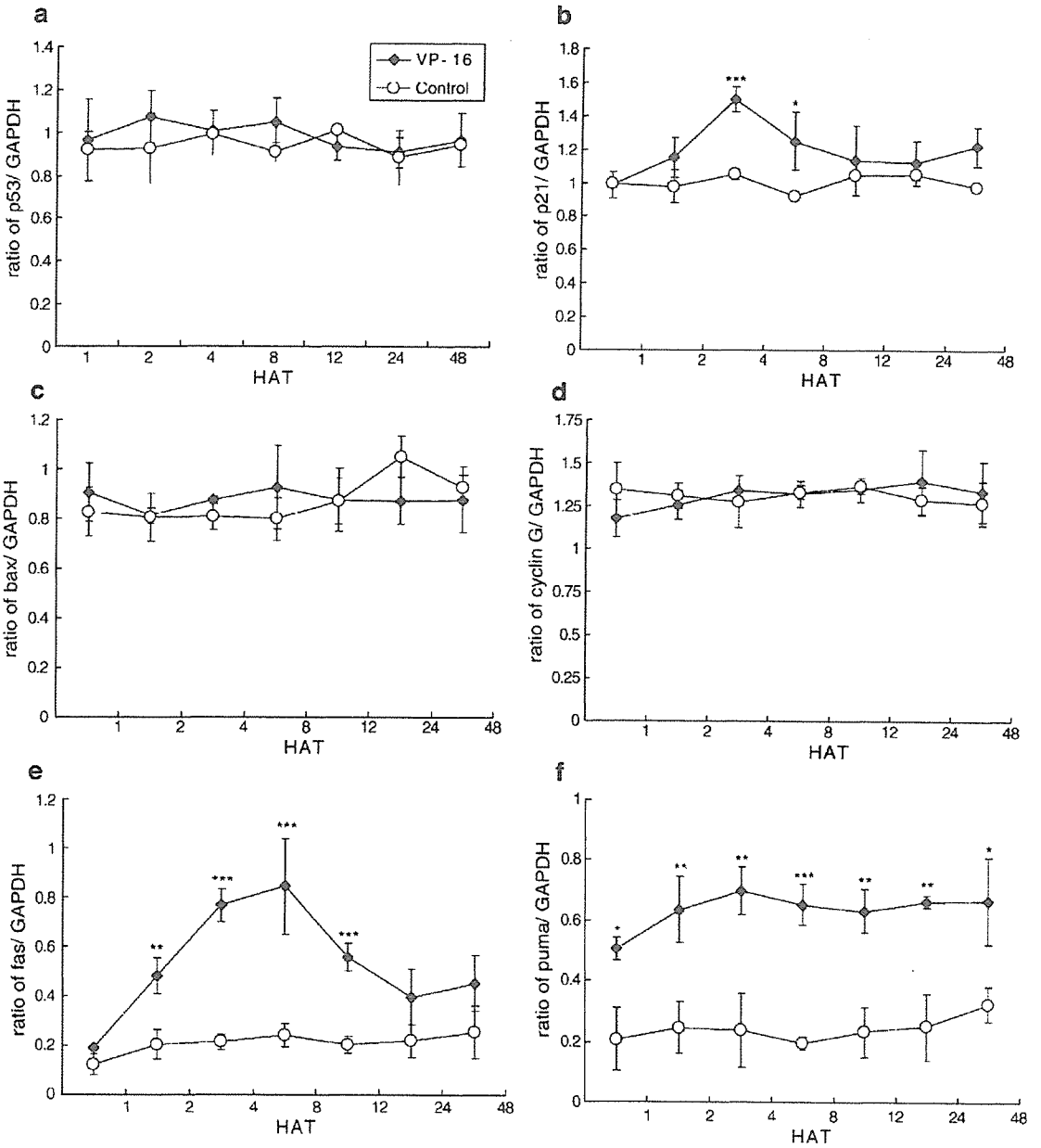

Fig. 4. Changes in the expression of *p53* (a), *p21* (b), *bax* (c), *cyclin G* (d), *fas* (e), and *puma* (f) in the brains of mouse fetuses exposed to VP-16. Each value represents the mean±S.D. of 6 fetuses from each dam. $^{*}p<0.05$, $^{**}p<0.01$, $^{***}p<0.001$: significantly different from controls by Student's *t* test.

2.6. Flow cytometric analysis

For cell cycle analysis, telencephalons of three fetuses from each dam were obtained in Hanker's balanced salt solution. Cells from the telencephalons were washed in PBS, and resuspended in 1 ml of PBS at a density of 1×10^6 cells/ml. Ice-cold ethanol (2.7 ml) was added to yield a final ethanol concentration of 70%. After centrifugation, the cells were resuspended in 1 ml of PBS and incubated with 10 μl of RNAse at 37 °C for 40 min. Ten microliters of propidium-iodide (5 mg/ml) were added. Forward scatter (FSC) and side scatter (SSC) analysis was performed to assess changes in cell morphology, and fluroscent lamp-2 height (FL-2H, red fluorescence) analysis to detect changes in cellular DNA content and DNA fragmentation using a FACSCalibur Flow Cytometer (Becton–Dickinson, Franklin Lakes, NJ). Using the Cell Quest program (Becton–Dickinson), doublets and debris were discarded and then the percentages of cells in the various phases of cell cycle were calculated.

3. Results

3.1. TUNEL

Pyknotic cells in the telencephalon of VP-16 treated mice began to increase at 4 HAT, peaked at 12 HAT, gradually